NATIONAL ADVISORY COMMITTEE FOR AERONAUTICS

TECHNICAL NOTE 2995

NEW EXPERIMENTS ON IMPACT-PRESSURE INTERPRETATION IN SUPERSONIC AND SUBSONIC RAREFIED AIR STREAMS

By F. S. Sherman

University of California

Washington
September 1953

NATIONAL ADVISORY COMMITTEE FOR AERONAUTICS

TECHNICAL NOTE 2995

NEW EXPERIMENTS ON IMPACT-PRESSURE INTERPRETATION IN SUPERSONIC AND SUBSONIC RAREFIED AIR STREAMS

By F. S. Sherman

SUMMARY

Results are presented of an experimental investigation of impact-pressure interpretation in supersonic and subsonic rarefied air streams at Mach numbers from 0.1 to 0.7 and 1.7 to 3.4 and in the Reynolds number range from 2 to 800. A study of the effects of impact-probe size on the accuracy of pressure measurements indicated that corrections for viscous effects are less than 1 percent for probes in supersonic flows at Reynolds numbers above 200, where the Reynolds number is based on the velocity, density, and viscosity of the free stream, the reference dimension being the outer diameter of the probe. Viscous-effect corrections are presented for interpretation of pressure measurements at lower Reynolds numbers.

INTRODUCTION

Measurements of impact pressures for the determination of the speed of an air stream require special interpretation when the Reynolds number based on probe diameter is less than about 200. The problem of this interpretation for the case of a probe at zero angle of attack in a rarefied gas stream has been the subject of several theoretical and experimental investigations (refs. 1 to 6). The results of the experimental portion of this work, as represented by reference 1 (supersonic flow) and reference 2 (subsonic flows), have to date been labeled tentative or preliminary but have served to indicate, for one type of impact probe, the nature and approximate magnitude of viscous effects. For supersonic flows the results served to identify a rough value of the Reynolds number above which viscous effects on this probe type were negligibly small. This value was $Re \approx 100$, where the Reynolds number is based on the velocity, density, and viscosity of the free stream and the outer diameter of the impact probe.

As a conclusion to both references 1 and 2, a need was expressed for further tests to cover wider ranges of Mach and Reynolds numbers. The present report describes experiments designed to provide these extended ranges, to include a limited study of the effects of impact-probe geometry, and to check on and to refine the results of the earlier work. The nature of these experiments and of their results has suggested an organization of the report in two main sections, a principal section presenting very briefly the information necessary for the correction to 1-percent accuracy of impact-pressure measurements in a uniform free stream, and an appendix giving the remaining details of method, technique, and results of interest in a further pursuit of the impact-pressure problem (appendix A). Additional appendixes describe key pieces of equipment which were designed for these experiments and some preliminary results of tests in a new nozzle which produces isentropic flow (appendixes B to D).

This work was conducted at the University of California under the sponsorship and with the financial assistance of the National Advisory Committee for Aeronautics.

SYMBOLS

C_μ dimensionless coefficient of viscous effect on impact pressure, $\dfrac{p_i - p_{i(ideal)}}{\frac{1}{2}\rho V^2}$

C_{μ_2} same coefficient, referred to dynamic pressure after a normal shock wave

d impact probe diameter, in.

$f(M)$ function defined by equation (5)

$g(M)$ function defined by equation (7)

h height of mercury column in McLeod gage capillary, in.

K numerical constant

M Mach number

n number of observations of a pressure

p pressure, μ Hg

p_i impact pressure, μ Hg

$p_{i(ideal)}$	impact pressure in an ideal, inviscid fluid, μ Hg
p_o	stagnation-chamber pressure, μ Hg
p_s	free-stream static pressure, μ Hg
p_2	cone surface pressure, μ Hg
Re	Reynolds number, based on probe diameter and free-stream velocity, density, and viscosity
Re_2	Reynolds number based on velocity, density, and viscosity after a normal shock
T	static temperature of free stream, ^{o}F abs
T_o	stagnation temperature, ^{o}F abs
V	velocity of free stream
γ	ratio of specific heats, 1.400 for air
ϵ	probable error in a pressure measurement, μ Hg
μ	viscosity of air at free-stream temperature, lb-sec/sq ft
ρ	free-stream density

EXPERIMENTAL METHOD

Since no independent, absolute method of calibrating the velocity of a supersonic low-density air flow had been developed,[1] the experimental method was based on a comparison of the performances of different-sized impact probes in a given air stream. References 1 and 2 describe two different techniques of utilizing the comparative pressure measurements. The technique applied in this work is the "extrapolation technique" of reference 2. For subsonic flows a suitable independent calibration of the jet was obtained by assuming an isentropic acceleration from its measured stagnation properties. In either type of flow the aim of the calibration is to find the Mach and Reynolds numbers of the test and to determine the value which the impact pressure would have if the

[1]A supersonic nozzle has now been designed which produces isentropic flow, giving an independent calibration. (See appendix D.)

flow were essentially inviscid. The experimental results consist of the relation between this inviscid (or ideal) impact pressure and the measured impact pressure, as a function of Re, M, and probe geometry.

EXPERIMENTAL APPARATUS

The tests were conducted in an open-jet, continuous-flow, nonreturn-type wind tunnel (no. 3 wind tunnel, ref. 7). The air flow initiates in the room, passes through driers where the dew point is lowered to about -25° F, through a Rotameter and metering valves, into the stagnation chamber. In this chamber the stream is broken up by baffles and screens and has an average speed which is less than 21 feet per second, according to the throat diameter of the nozzle. The dynamic pressure of the flow in the stagnation chamber is always less than 0.023 percent of the measured pressure at a wall opening in the chamber. Acceleration and expansion of the flow to the desired supersonic or subsonic stream conditions were produced by appropriate nozzles. The nozzles used were all axisymmetrical, those producing supersonic flow being designed by a method presented in reference 8 and the one for subsonic flow being a 9-inch-throat-diameter International Standards Association nozzle (ref. 9). The diameter of approximately uniform flow varied from 2 to 4 inches in supersonic flows and from 4 to 7 inches in subsonic streams. Downstream of the test section the stream passes through a large manifold chamber to the intake of the stream-drive ejectors which recompress the air and discharge it to the atmosphere.

The impact probes under test were mounted on an eight-faced rotary probe selector which is described in appendix C. Thus a maximum of eight impact probes could be tested consecutively in a given flow or series of flow conditions, without need to open the tunnel test section, compared with a maximum of two probes in the experiments of reference 1 and three in those of reference 2.

All pressure measurements involved in the experiments were made either with a precision U-tube manometer (ref. 10) with n-butyl phthalate as the fluid or with a special mercury McLeod gage which is described in appendix B.

Three types of impact tubes were tested. Two of these had the external geometry of an incompressible source-shaped body, differing from each other in the relative size of the impact-pressure orifice. The third was a straight, sharp-lipped cylinder. These shapes are shown in figure 1. Reference 1 gives typical coordinates for the source-shaped profile. The three types will be designated as A, B, and C, as shown in figure 1.

RESULTS

For the purpose of correcting impact pressures measured with probes of type A, B, or C to an accuracy of ±1 percent, the results of the present experiments are shown graphically in figures 2 and 3.

For use of the probe in a supersonic air stream, one graph for each probe type shows the ratio of the measured impact pressure to the ideal or nonviscous impact pressure plotted against the Reynolds number based on probe diameter and free-stream properties. This presentation is not particularly suited to a comparison between theory and experiment but is easy to use and has the advantage of causing a partial collapse of the Mach number dependence of the impact-pressure correction for $1.5 < M < 3.5$.

A different presentation of results is necessary in the case of subsonic impact pressures. In it a dimensionless pressure coefficient is formed from the difference between measured and ideal impact pressures divided by the dynamic pressure $\frac{1}{2}\rho V^2$ of the free stream. Since no systematic Mach number influence was detectable in a plot of this quantity against the Reynolds number, the performances of the two types (B and C) which were tested subsonically are shown in the same graph (fig. 3).

In each of figures 2 and 3 a dashed line has been drawn by eye, indicating the best average impact-pressure correction for the entire present range of test conditions.

COMPARISON WITH EARLIER EXPERIMENTAL RESULTS

Figure 4 shows the comparison between the present results for type B probes in supersonic flow with those of reference 1, over their common Mach number range (nozzles 2A and 3, $2.3 < M < 3.4$). The check on these earlier results is seen to be very good.

Figure 5 shows the corresponding comparison between the present results and those of reference 2 (subsonic flows) when the stagnation-chamber pressure is taken as the ideal impact pressure in analyzing both sets of data. In the same graph the much earlier results of Homann (spherical-headed impact tubes in oil channel, ref. 11) and of Barker (straight cylindrical tubes in water pipe flow, ref. 12) are indicated by curves fitting their data.

CONCLUDING REMARKS

Tests have been completed which yield experimental corrections to the measured values of impact pressure at low Reynolds numbers in both supersonic and subsonic air streams. The corrections were determined for three different shapes of impact probe in supersonic flows and for two shapes in subsonic flows, the probes being set at zero angle of attack in a uniform air stream. The corrections apply directly in the ranges $1.7 < M < 3.4$, $15 < Re < 800$ and $0.1 < M < 0.7$, $4 < Re < 300$, where the Reynolds number is based on the velocity, density, and viscosity of the undisturbed free air stream and on the outer diameter of the impact probe. For $Re > 200$, the correction amounts to less than 1 percent of the impact pressure except at the highest speed subsonic flows.

The agreement between experimental results and theoretical predictions (discussed in detail in appendix A) is fair, becoming better as the boundary conditions of the theories more closely approximate those of the experiment.

The experimental results did not determine whether or not slip or other rarefied-gas phenomena are important within the present ranges of M and Re.

University of California,
Berkeley, Calif., June 20, 1952.

APPENDIX A

DETAILED DISCUSSION OF EXPERIMENTAL PROCEDURE AND RESULTS

INTRODUCTION

The main section of this report has described only the gross aspects of the present experiments and of their results. The purpose of this appendix is to describe and discuss in greater detail certain interesting smaller scale characteristics of the experimental results, which were clearly enough detectable within the limits of experimental accuracy but which could not be correlated for easy use in impact-pressure corrections. Also, since a relatively high degree of accuracy of measurement is claimed for these experiments, a full statement of the experimental technique and precautions is given along with a critical discussion of the method of analysis of the data.

EXTRAPOLATION TECHNIQUE FOR DETERMINING IDEAL IMPACT PRESSURE

In the experiments on impact pressures in supersonic air streams, the critical problem in the experimental method was that of inferring the value of the ideal impact pressure at a given flow setting from a comparison of the measured values obtained with a number of different impact probes. The technique employed was essentially the same as that used in reference 2. For a number of probes of the same shape, the procedure consists of plotting the measured impact pressures against the inverse of impact-probe diameter and extrapolating a curve through the resulting points to $1/d = 0$. The value of the pressure intercept at this point is taken to be the ideal impact pressure. The process of letting $1/d$ approach zero is considered equivalent to letting the Reynolds number approach infinity, all other factors in Re having been held constant.

This method of attack seemed quite reasonable at the time of writing of reference 2 and appeared to be substantiated by both theory and preliminary experiments. Theory predicted, in particular, a nearly linear relationship between p_i and $1/d$, so that extrapolation should be possible to perform with ease and accuracy, especially if a fair number of points on the curve are known. Experiments in subsonic air streams appeared to confirm this linearity for a narrow range of quite small Reynolds numbers ($2 < Re < 12$). However, in the current experiments, particularly at the higher supersonic Mach numbers and Reynolds numbers where the effect of viscosity on p_i was proportionally small, curves of p_i against l/d were pronouncedly nonlinear in many cases, often having a shape which made extrapolation to an intercept very difficult and inaccurate (see fig. 6). This pointed out the necessity for cautious procedure in cases where there remains a significant gap between the Reynolds number of the largest probe being compared and the Reynolds number above which viscous effects are no longer detectable.

The necessity of improving the accuracy of the extrapolation procedure was the primary reason for testing more than one type of impact probe. While the curves of p_i against l/d for probes of two different shapes in the same air stream would in general be expected to be different, they should tend to converge on the same p_i intercept at $l/d = 0$. This requirement is in effect a hypothesis based on the observation that impact probes of all shapes sense very nearly the same pressure when at zero angle of attack in a stream of negligible viscosity. With the three probe types used the procedure was to test a sequence of five or six probes of each type at each condition of the wind-tunnel jet, plot all the data together as curves of p_i against l/d, and then attempt to reconcile the results in terms of three curves having the same $p_{i(ideal)}$ intercept and passing through the three sets of points. The resulting picture may be seen for a few cases in figure 6. (Actually, it was not possible to test all these probes in the identical air stream, but a satisfactory accounting for the small discrepancies involved in resetting wind-tunnel flow conditions was made, as explained in a later section.)

Finally, a type of iteration process was employed to refine the determination of the intercepts. When the data for all runs and probe types had been reduced, in terms of the first guesses at intercepts, to yield curves of $p_i/p_{i(ideal)}$ against l/Re over the entire range of Reynolds number, these curves served to indicate somewhat further the correct shape of curve to draw for extrapolation purposes. Also in cases where a slight change in the intercept removed an otherwise unexplainable bit of scatter from the curves over the entire Reynolds number range, this change was made. Inasmuch as the extrapolation technique of data reduction is from the start an indirect one, it seems justifiable to manipulate it in this way, always aiming toward the most consistent picture of the experimental results as a whole.

In the tests in subsonic streams, this problem did not occur, or rather it was avoided by assuming the stream to be isentropic in its flow from the stagnation region, since the extrapolated values of $p_{i(ideal)}$ were in excellent agreement with the measured values of the stagnation-chamber pressure.

EXPERIMENTAL TECHNIQUE AND PRECAUTIONS

Equipment

Uniformity of wind-tunnel air streams.- Before performing the comparison tests of impact tubes, the supersonic and subsonic jets were surveyed with impact and static-pressure probes to determine the general extent of their uniform flow regions and the magnitude and character of local nonuniformities in the immediate vicinity of the position of the test probes. The subsonic jet was found to be uniform (within the sensitivity of the instruments) over a core of diameter from 4 to 7 inches. The supersonic jet cores varied in diameter from 2 to 4 inches, and the radial variations of impact pressure at the nose of the test probes are shown in figures 7(a) to 7(c). These were measured at the time of the tests with a 0.300-inch-diameter type B probe.

Size range of impact probes.- The largest diameter of test probe used was 0.600 inch with supersonic nozzles 2A and 3, 1 inch with supersonic nozzle 6, and 1.500 inches with the subsonic nozzle. With this size choice no evidence of blocking of the supersonic jets was detected, whereas the subsonic jet evidenced blocking for any probe. The probes for use in supersonic jets were 4.5 inches long; those for subsonic jets were made 9 inches long, after tests showed that 13-inch-long probes afforded no essential relief of the jet blocking effect. The minimum allowable diameter was either 0.10 or 0.15 inch, as determined by the time-response and outgassing equilibrium characteristics of the probe and pressure-measuring system. Figure 8 shows representative groups of the impact probes used in supersonic and subsonic air streams.

Static-pressure probes.- The static pressure of the supersonic jet was determined with the aid of a 5° semiapex angle cone probe. This probe and its use are described in reference 7. To measure the static pressure of the subsonic jet, a probe was constructed according to the design shown in figure 9. This probe was used only to demonstrate the constancy of static pressure across the subsonic jet, after which static pressures were measured with a throat tap in the nozzle.

Procedure

Leak testing.- All probes were determined to be free from leaks, before installation, by use of a helium mass spectrograph-type leak detector. The entire pressure-measuring system, including the rotary probe selector, was similarly carefully leak-tested after assembly. In addition, further tests were performed during the course of the experiments whenever the data suggested the possibility of a leak.

Time-response testing of probes.- Each probe, with the associated manometer and connecting tubing, was tested for its time response to a very rapid pressure rise in the wind tunnel from a fraction of a micron of mercury to about 230 microns of mercury. Records of the pressure rise in the probe-gage system for the various probes were obtained by use of a thermistor Pirani gage (Western Electric type D176255) and a millivolt chart recorder. The time required for the recording of 99.9 percent of the pressure increase varied from several seconds to several minutes. No probe was used for which this time was more than 10 minutes, or for which the equilibrium pressure in the gage system differed measurably from that in the tunnel.

As an added precaution during the actual measurements of impact pressures the thermistor gage was left installed and provided direct evidence of steady-state conditions at each measurement.

Calibration of U-tube manometer.- The U-tube manometer was calibrated by comparison with the McLeod gage in the range from 0 to 850 microns, as described in reference 10. In addition, a precise specific-gravity determination was run on a carefully outgassed sample of the manometer oil at 71° F. The degree of agreement between the results of these two methods is discussed in appendix B.

Impact-probe comparison tests.- The impact probes to be compared during a given run were placed successively at a specified point in the air flow, usually on the nozzle center line. After a suitable wait for equilibrium in the gage system, the pressure sensed by the probe was measured by the manometer or McLeod gage. After each probe had been tested in turn, the cycle would be repeated to obtain an estimate of the reproducibility of the data, except in cases involving the McLeod gage, where time limitations prohibited this repetition.

In the tests in subsonic flow the throat-tap static pressure was measured with each impact pressure, since the throat static pressure varied with the size of the probe in the stream. In the supersonic flow work occasional measurements were made of the pressure in the test chamber surrounding the fluid stream.

In the last third of the work with supersonic streams, and in all the work with subsonic flow, the stagnation-chamber pressure was measured at each different flow setting. The stagnation temperature (approximately room temperature) was measured for each flow setting throughout the entire experiment.

REDUCTION AND ANALYSIS OF DATA

Extrapolation Procedure

A general description of the nature and difficulties of the extrapolation technique of analyzing these comparison-type data was given in an earlier section. The present section serves to describe the use of "reference probes" to coordinate the data taken with the three types of impact probe when there appeared significant discrepancies in the reproduction of flow conditions between runs. Supposing that three runs were required to test all probes at a given flow setting, one reference probe would be common to all three. The difference between its readings during the first run and either of the subsequent runs would simply be added to or subtracted from all impact pressures of the later run. This procedure seemed adequate for the small adjustments involved. The extrapolation curves were then drawn from these adjusted pressures, as shown in a few samples in figures 6 and 10.

Calculation Formulas

Supersonic flow.- Given $p_{i(ideal)}$, the surface pressure on the conical probe p_2, and the stagnation temperature T_o, the Mach number and Reynolds number are computed as follows:

The Mach number M is a tabulated function of the ratio $p_{i(ideal)}/p_2$, as explained in reference 7.

The true static pressure p_s is a tabulated function of M and p_2 (ref. 13).

The free-stream temperature is calculated from T_o, M, and the assumption of adiabatic flow from the stagnation chamber:

$$T = T_o\left(1 + \frac{\gamma - 1}{2} M^2\right)^{-1} \qquad (1)$$

The viscosity of air at temperature T is taken from reference 14.

The Reynolds number is calculated from the preceding quantities and the outside diameter of the impact tube (the asymptotic diameter in the case of source-shaped profiles), with the formula (the form of which is derived in ref. 7)

$$\mathrm{Re} = 6.63 \times 10^{-6} \frac{Mp_s d}{\mu\sqrt{T}} \tag{2}$$

The units of p_s, d, T, and μ are as given in the list of symbols, and the density of mercury is taken to be 13.54 grams per cubic centimeter.

The viscous effect on a measured impact pressure is probably best characterized for detailed study and comparison with theory by the dimensionless pressure coefficient C_μ defined by the equation

$$C_\mu = \frac{p_i - p_{i(ideal)}}{\frac{1}{2}\rho V^2} = \frac{p_i - p_{i(ideal)}}{\frac{1}{2}\gamma p_s M^2} \tag{3}$$

Actually the dynamic pressure which occurs in the denominator was calculated from a tabulated relation between $p_{i(ideal)}$, M, and $\frac{1}{2}\rho V^2$ (ref. 15 and fig. 11).

So far all the properties taken to characterize the air stream are those of the undisturbed free stream. It is frequently of interest to have another set of reference properties, those resulting when the free stream is assumed to have passed through a normal shock wave. These were calculated by the use of tables (ref. 15) of normal shock functions for a nonviscous fluid and are identified in this report by the subscript 2. Some results of this calculation should be noted for a ready understanding of the relation between final graphs of $p_i/p_{i(ideal)}$ or C_μ against Re and of C_{μ_2} against Re_2, since at a casual glance these various plots might seem to indicate contradictory trends of viscous effect as an explicit function of the Mach number. The result in point is represented by the equation

$$\left(C_\mu\right)(\mathrm{Re}) \equiv \left[f(M)\right]\left(C_{\mu_2}\right)\left(\mathrm{Re}_2\right) \tag{4}$$

where by the definitions of C_μ and Re, and by the laws of flow through a normal shock wave,

$$f(M) = \left(\frac{\mu_2}{\mu}\right)\left(\frac{V_2}{V}\right) \tag{5}$$

In the plot of $f(M)$ shown in figure 12 the point of interest is the existence of the minimum, which occurs within the operating range of nozzle 2A, while nozzles 3 and 6 operate at nearly equal intervals to the right and left of the minimum, respectively.

If the results are presented in terms of the ratio $p_i/p_{i(ideal)}$ instead of C_μ, the picture changes once again. This change is expressed in the equation

$$p_i/p_{i(ideal)} = 1 + g(M)C_\mu \tag{6}$$

where

$$g(M) = \frac{1}{2}\rho V^2 / p_{i(ideal)} \tag{7}$$

A plot of $g(M)$, showing the operating ranges of the three nozzles, is given in figure 13.

In order to illustrate and emphasize the point of this discussion, figures 11(a) to (c) have been included. They show the appearance, in each of three presentations, of the simple expression $C_{\mu_2} = 16/Re_2$ (the result of theory for a source-shaped probe in incompressible flow). Assuming this expression to give the correct description of affairs behind a normal shock for a probe in supersonic flows,

$$C_\mu = f(M) \times \frac{16}{Re}$$

and

$$p_i/p_{i(ideal)} = 1 + g(M)f(M) \times \frac{16}{Re}$$

Figures 11(a) and 11(b) show plots of C_{μ_2} against $1/Re_2$ and of C_μ against $1/Re$. Figure 11(c) shows a plot (to the same scale as those of figs. 2(a) to 2(c)) of $p_i/p_{i(ideal)}$ against Re. The function $f(M) \times g(M)$ has a minimum at $M \approx 2.1$.

A similar example could be carried out for a case in which C_{μ_2} decreased monotonically with M at constant Re_2 and would show a quite different (in particular, nonmonotonic) appearing Mach number dependence in C_μ or in $p_i/p_{i(ideal)}$ at constant Re. This example gives an approximation to the present experimental results.

Subsonic flow.- A few modifications of this data-reduction scheme were made for the analysis of the data taken in subsonic jets. They were largely dictated by the amount of data scattering due to drift in ejector performance and by an attempt to compensate for interference or blocking effects which differed from probe to probe. Fairly satisfactory results were achieved by handling the data in terms of the ratio of p_i to p_s instead of in terms of these pressures individually. It appeared that blockage effects caused roughly equal increments in p_i and p_s, and, since p_i and p_s were nearly equal in subsonic flow, their ratio would be relatively unchanged. This was especially true at the lowest Mach numbers, where the greatest accuracy of determination of p_i/p_s is required to assure reasonable accuracy in M. In addition, the pressure fluctuations from the ejectors seemed to have rather low frequencies, so that the p_i and p_s readings taken for a given probe with about 5 minutes intervening between them would represent a fairly constant operational pressure level, whereas the same two readings taken an hour later would each have risen a fraction of a percent. The ratio of p_i to p_s, however, would have changed much less. The magnitude of all these effects is best seen in table I.

Moreover, when the extrapolation procedure was carried out on the basis of p_i/p_s against $1/d$, such good agreement was found with an average value of p_o/p_s that it was considered adequate to take $p_{i(ideal)}$ and p_o to be the same. This amounts to assuming isentropic flow from the stagnation chamber to the impact probe.

According to these considerations, the data reduction was completed as follows:

$$M = \left\{\frac{2}{\gamma - 1}\left[\left(\overline{\frac{p_o}{p_s}}\right)^{\frac{\gamma-1}{\gamma}} - 1\right]\right\}^{1/2} \tag{8}$$

where the bar over any quantity indicates an arithmetic mean of all its measured values. With this value of M and the measured or computed values of T_o, $\overline{p}_o$, $\overline{p}_s$, and p_i the Reynolds number and the pressure coefficient C_μ were computed by formulas equivalent to equations (2) and (3):

$$Re = 6.63 \times 10^{-6} \frac{M\bar{p}_s d}{\mu\sqrt{T}} \tag{9}$$

$$C_\mu = \frac{1}{\frac{\gamma}{2} M^2}\left[\frac{p_i}{p_s} - \left(\frac{\bar{p}_o}{p_s}\right)\right] \tag{10}$$

If no temporal pressure changes or blocking effects had occurred, these equations would reduce identically to equations (2) and (3).

EXPERIMENTAL ERROR

Supersonic Flow

Pressure measurements.- All pressure measurements were taken with the U-tube manometer. By a comparison of the calibration data of this instrument with data from the new McLeod gage, the probable error of a given pressure measurement with the manometer was estimated to be ±0.00038 inch of n-butyl phthalate. This estimate was obtained from the formula (ref. 16)

$$\epsilon = \frac{0.6745}{\sqrt{n - 1}}\left[\sum_{K=1}^{n} \left(p_K{}^* - p_K\right)^2\right]^{1/2} \tag{11}$$

where n is the number of measurements during a calibration run, p is the manometer reading, p^* is what the manometer should read at that pressure according to the best straight line fitted through the calibration data, and ϵ is the probable error of the reading p.

(1) Impact pressure: According to the above result the proportional probable error in p_i varied between 0.3 percent at the lowest p_i to 0.04 percent at the highest p_i.

(2) Cone surface pressure: By the same reckoning the proportional probable error in p_2 varied between 2.1 and 0.3 percent. There is, however, another major source of error in p_2 which is limited to a

theoretical estimate at this time. This is the effect of low Reynolds number on the cone surface pressure p_2, which is analyzed approximately in reference 17. According to reference 17, this effect can amount to about 5 percent of p_2. No experimental evidence is at hand to support this estimate, however, since the difficulties of a comparison-type experiment are greater for the cone static probes than for the impact probes. It is necessary, therefore, to regard this element of uncertainty in the experiments as unknown.[2] With regard to the effect which this possible error might have on the final picture of the experimental results, a recalculation of all results including a correction to p_2 as given by the theory of reference 17 indicated that the corrected curves differed from the uncorrected ones only by an amount less than the uncertainty of drawing either set.

(3) Ideal impact pressure: The probable error in $p_{i(ideal)}$ varied between 2 to 5 microns (0.8 to 0.2 percent, the higher value occurring at the lowest impact pressures). These estimated values were derived from a graphical study of the extrapolation curves. An attempt to perform the extrapolations analytically was abandoned as lacking sufficient generality and theoretical basis.

Mach number, Reynolds number, and C_μ.- The probable errors in Mach number, Reynolds number, and C_μ are as follows:

(1) Mach number: According to the estimated values of probable error in $p_{i(ideal)}$ and p_2 (ignoring the possibility of viscous effects on p_2), the probable error of the ratio of $p_{i(ideal)}$ to p_2 varies between 2.3 and 0.4 percent, corresponding to a probable error in M of 1.5 to 0.3 percent.

(2) Reynolds number: Aside from possible errors in the assumption of adiabatic flow from the stagnation chamber to the test point in the nozzle, or in the viscosity data, the error in Re was an accumulation of those in p_s, M, d, and T_o. Taking probable errors of 0.5 percent

---

[2] Recent experimental results in the new isentropic-flow nozzle for $M = 4.00$ have shown the error in p_2 to be even more serious, being on the order of 20 percent. The resulting error in M was about -10 percent, but the errors in dynamic pressure and Reynolds number were much smaller (<3 percent) because of a cancellation of effects. A detailed experimental investigation of cone probes is now under way in the no. 3 wind tunnel, but it is not expected that the results of this program will seriously invalidate the impact-pressure data as they are presented here.

in d and of 0.2 percent in T_o, there results a probable error in Re varying from 3.5 to 0.8 percent.

(3) C_μ: The probable error in C_μ was governed primarily by the error in $p_{i(ideal)}$ and ranged from 0.003 for the highest rate of flow in nozzle 6 to 0.017 for the lowest flow rate in nozzle 2A. Results on type C probes in nozzles 2A and 3 may be somewhat more uncertain than this, since these probes were most influenced by the relatively large local nonuniformities of flow in these nozzles.

Subsonic Flow

Pressure measurement with McLeod gage.- Pending more precise measurement of the capillary diameter and compression volume, the probable error in gage readings converted to pressure is about 1 percent. The probable error in the ratio of two nearly equal pressures, in terms of the sensitivity of the McLeod gage, is of major interest. If Δh is the probable error in any height h of mercury in the McLeod gage capillary, the probable error in h^2 is $2h\,\Delta h$. The ratio of two pressures p_a and p_b is essentially the ratio of ${h_a}^2$ to ${h_b}^2$. If $h_a \approx h_b \approx h$, then the probable error in this ratio is $2\sqrt{2}\,\Delta h/h$. For the precision McLeod gage, a reasonable estimate of Δh is 0.001 inch. If this value is used, the probable error in the ratio of p_a to p_b ranges from 0.12 percent to 0.03 percent as p ranges from 35 to 850 microns, the extent of the present use of the instrument.

Pressure measurement with manometer.- The manometer was employed for pressures from 850 microns to 3,250 microns. In this range it yielded the ratio of two nearly equal pressures with a probable error running from 0.13 to 0.03 percent.

Mach number.- The uncertainty in M resulting from the probable error in the ratio $\overline{p_i/p_o}$ depends upon both the nominal value of M and the pressure level. The results of a few limiting case calculations are shown below:

p_s, microns	M	Probable error in M, percent
1,800	0.100	±4.0
3,250	.100	±2.5
35	.600	±.2
400	.600	±.05

In many cases these errors may look unbelievably small, and it should be emphasized that they reflect only the precision of pressure measurement and include no estimate of the validity of isentropic-flow theory in this application and so forth. In particular it is quite impossible to estimate accurately the amount of change in M during tests in which it was nominally constant but in which blocking effects varied from probe to probe.

Reynolds number.- The probable error in Re amounts to about 1.5 percent more than that in M, because of the additional quantities involved in Re; thus it ranges between extreme values of 1.5 to 6 percent.

C_μ.- The major contributions to the error in C_μ came from the errors in the ratios p_i/p_s and $\overline{p_o/p_s}$. Since the difference in these two ratios was usually very small, the proportional probable error of the difference was often quite large. The easiest way to describe the magnitude is by reference to figure 14, where each value of C_μ is surrounded by a circle or a square, the radius or $\frac{1}{2}$- edge length of which indicates the probable error for that value. The very large errors near the origin come from the difficult measurements at very low Mach numbers.

DISCUSSION OF EXPERIMENTAL RESULTS

Correlation of Results for Detailed Study

In the section "Reduction and Analysis of Data" various alternative presentations of the final results of these experiments were indicated and related to one another. A unified and detailed study of the entire experiment is possible when C_{μ_2} is plotted against $1/Re_2$ for data taken in supersonic flows and C_μ is plotted against $1/Re$ for subsonic flows. This procedure has the advantage of allowing a direct comparison of the test results from supersonic and subsonic air streams and the most direct correlation with existing theories (e.g., refs. 5 and 6). A further empirical advantage is evident in that both theory and experiment indicate very little explicit dependence on M of such plots for probes in a uniform subsonic stream, while the same plots for probes in a supersonic free stream show a fairly uniform dependence on M (as should be expected from the effect of the detached shock wave). In the section "Reduction and Analysis of Data" it was shown that the correlations based on free-stream properties of the supersonic stream will not have this last property throughout the present Mach number range.

With reference to alternative methods of correlating the data, it should be remarked that the plotting of $p_i/p_{i(ideal)}$ against M/Re, which appeared quite successful in reference 1, broke down when new data at lower Mach numbers were included. The presentation of final results in reference 2 also seems faulty, since the graph gives $\left(p_i - p_{i(ideal)}\right)/p_s$ as a function of M^2/Re, with a resultant implication of slip flow through the use of the latter parameter. Actually, the M^2 belongs not over the Re in the abscissa but with the p_s in the denominator of the ordinate, where it makes up (except for the factor $\gamma/2$) the dynamic pressure $\frac{1}{2}\rho V^2$.

Comparison of Experiment and Theory

The final graphs of C_{μ_2} against $1/Re_2$ are shown in figures 15(a), 15(b), and 15(c) for type A, B, and C probes, respectively. For types B and C the same scales are used to show C_μ against $1/Re$ for these probes in subsonic flows. The results of various theoretical calculations are compared graphically with one another in figure 16. The theories compared are:

(a) A stagnation line analysis for a source-shaped probe in an incompressible, slightly viscous fluid (ref. 6)

(b) A similar analysis for a hemispherical-headed probe in a compressible (subsonic), slightly viscous fluid, including (ref. 5) and excluding (ref. 4) the possibility of slip at the boundary

(c) A stagnation line analysis for the source-shaped probe in a very viscous, incompressible fluid (ref. 6)

None of these theories pretends to offer an accurate prediction of the present experimental results, even for subsonic air streams, since their treatments of viscosity and compressibility effects are all very approximate and since the geometrical boundary conditions employed are not those encountered in the experiment, making no allowance for the presence of the impact-pressure orifice. One possibly significant result to notice is the manner in which the introduction of the slip boundary condition in reference 5 largely destroys the dependence of C_μ on M which was predicted in the case of no slip (ref. 4). No systematic explicit variation of C_μ with M was observed in the experiments in subsonic streams, although the probable error in the experimental values of C_μ would make it difficult to define even the Mach number dependence suggested by reference 4. (This lack of an explicit dependence of C_μ

on M explains the use, in figs. 15(b) and 15(c), of a single symbol to represent all subsonic data.)

To orient these theoretical results with respect to the present empirical data the curve for the first-mentioned theory has been drawn in figures 15(a) to 15(c). The theories for a slightly viscous fluid give curves lying above the data for all three types of probe (except for a few points), particularly for the data taken in supersonic flow. (This is only apparently in disagreement with the comparison between experiment and theory shown in ref. 1 where eq. (2) and figs. 12 and 13 are in error, in that the Reynolds number in eq. (2) is based on the radius of the impact tube instead of the diameter as stated. The correct equation referred to the diameter of the impact tube is

$$\frac{p_i}{p_s} = \left(\frac{p_i}{p_s}\right)_{\text{Rayleigh}} + \left(\frac{2\gamma}{\gamma - 1} M^2 - \frac{\gamma - 1}{\gamma + 1}\right)\frac{\gamma M_1^2}{Re_1} \frac{2\phi_1}{1 + \frac{K_1}{\sqrt{Re_1}}}$$

where in ref. 1 the subscript 1 refers to conditions behind a normal shock. Then, for a full sphere

$$\phi_1 \approx 3 - \frac{83}{110} M_1^2 \qquad K_1 = 0.643$$

and for the hemisphere attached to a cylinder

$$\phi_1 \approx \frac{29}{8} - \frac{31}{34} M_1^2 \qquad K_1 = 0.643$$

When this correction is made, the theoretical curves in figs. 12 and 13 are altered slightly in shape and shifted by a factor of 2 in the direction of higher Re, giving a comparison of theory and experiment which agrees with that shown in the present report.)

While the subsonic data showed no measurable explicit Mach number dependence, the curves of C_{μ_2} against Re_2 for the probes in a supersonic stream do show a fairly certain uniform trend with M, C_{μ_2} decreasing at a given Re_2 as M (free-stream) increases. These curves approach more closely to that giving the subsonic performance of the probe and to the theoretical estimates as the supersonic free-stream Mach number approaches 1. Since the physical picture on which the calculation of C_{μ_2} and Re_2 was based is that of a normal shock wave sufficiently detached to be free of any influence of the boundary layer on the probe, and since the bow shock wave associated with a blunt body in a supersonic stream becomes more nearly normal and more distantly detached as M approaches 1, the above result is quite reasonable. The trend of C_{μ_2} with M at constant Re_2 is shown in these graphs (figs. 15(a) to 15(c)) only as the average Mach number of one nozzle differs from that of the next but appears also throughout the variation of M obtained within the range of operation of each nozzle. The latter variation has not been indicated graphically because of the confusing complex of symbols necessary, but the result may be seen numerically in table II. For very small changes of M, the detection of a trend infringes on the limits of experimental error and scatter. The most glaring exception to the general trend is shown in figure 15(c), where the C_μ values for type C probes at the lowest flow rate in nozzle 2A lie far below all other results. There has not been an opportunity to repeat the measurements to check this discrepancy.

One of the results of the present experiments was the demonstration of the magnitude and character of the differences in viscous effects on the impact probes of different shapes. These differences are seen in the graphs and can be summarized roughly in the statement that, at constant M and Re, C_μ decreases as the ratio of impact-pressure-orifice diameter to outside probe diameter increases, even becoming negative in certain ranges of M and Re for type B and C probes. This relationship is true whether the probes are used in supersonic or subsonic flow, but it appears more distinctly in the former case. The frequency of occurrence of negative C_μ values among the data from subsonic flows is negligible.

As seen in figure 2(b), the magnitude of the "reversal" of viscous effects on the type B probes is always small, seldom amounting to more than 1 percent of p_i in the range of the experiments. This fact accounts for the lack of any mention of the phenomenon in reference 1, where it is noticeable in the data but was quite justifiably considered to be an anomalous behavior within the limits of experimental accuracy at that time. It should also be emphasized that the reality of this effect in the present experiments has been scrupulously criticized, especially to verify that the phenomenon is not merely a characteristic of the particular wind-tunnel setup. In particular, tests showing the strongest reversal were repeated with the probe located away from the nozzle axis, where the condition of local flow nonuniformities would be different from that existing at the axis, and where interferences between the probe and the jet boundary should be somewhat changed. The reversal appeared in these tests in a practically unchanged fashion.

The effects of probe geometry are especially pronounced in the Reynolds number region where viscous action is first noticeable. The performances of the three types of probe in this region may be somewhat unified if the characteristic length in Re is changed from the outside diameter of the probe to the diameter of the impact-pressure orifice. For instance, it is then possible to set a limiting value of this new Reynolds number above which C_μ will have no value greater or less than ± 0.01. This limiting Reynolds number is about 100 for the probes in subsonic flow and varies between 100 and 200 with increasing M for probes in supersonic flow.

As regards the comparison of experiment and theory, it is encouraging to see that the agreement between the two becomes better as the impact orifice becomes relatively smaller, since the boundary conditions for the theoretical calculations specify no hole at all.

A final word may be added in discussion of the significance of the theory of reference 6 for the performance of an impact tube in a very viscous fluid. This theory is based on a Stokes "slow flow" type of analysis and would be expected to have validity only for Reynolds numbers much smaller than those encountered in the present experiments. Somewhat surprisingly, this analysis yields the same type of dependence of C_μ on Re $\left(\text{i.e., } C_\mu \propto 1/\text{Re}\right)$ as does the theory for a slightly viscous fluid. Only the coefficient of proportionality is changed, having a lower value for the very viscous fluid. This apparently agrees with the observed dropping off of the curve of C_μ against $1/\text{Re}$ for the lowest Reynolds numbers of these experiments and of the work of reference 2, but it should be observed that this same sort of decline could be fitted theoretically by taking the characteristic dimension of the Reynolds number to be increased by some sort of boundary-layer thickness, so that for moderately large Re, $C_\mu \propto 1/\left(\text{Re} + K\sqrt{\text{Re}}\right)$. This is the procedure used by Homann (ref. 11) to provide an excellent fit to his data on the stagnation-point pressure on spheres in an incompressible viscous fluid.

APPENDIX B

A SPECIAL MCLEOD GAGE FOR PRESSURE RANGE

0 TO 850 MICRONS OF MERCURY

THE NEED FOR THIS INSTRUMENT

The work of reference 2 indicated that an unusual degree of precision in pressure measurement is needed to insure reasonable correlation of the viscous effects on impact probes in subsonic air streams. Specifically, an instrument which could yield the ratio of two nearly equal pressures with an accuracy of 0.1 percent in the pressure range $35 < p < 1{,}000$ microns was needed for the present experiments. No instrument previously available in this laboratory was capable of such precision and range.

GENERAL DESCRIPTION OF NEW GAGE

The type of gage chosen in an attempt to obtain this performance was a mercury McLeod gage, in which special arrangements for very accurate reading were incorporated. The general appearance of the gage 's shown in figure 17. The capillaries are of precision-bore tubing shrunk over selected 0.120-inch-diameter steel drill rod. The closed capillary is 11.5 inches long, the closed end being made by the sweating in of a square-ended plug. The compression volume is approximately 44.9 cubic inches (735 cubic centimeters). The mercury is raised in the gage by atmospheric air pressure, air for this purpose being drawn through a silica-gel drier. The mercury reservoir is of stainless steel, which was chosen to provide an economical shape, rigidity, and a flat bottom for the gage as a whole. Joints between the steel and glass are standard taper ground joints, with female members of Kovar. A small stainless-steel bellows is attached to the reservoir, providing for a very delicate final adjustment of the mercury level in the gage at the time of reading. Also included in figure 17 are the chassis and reading mechanism for the gage. Not shown in this photo is the liquid air trap through which the gage is attached to the source of the pressure to be measured.

READING MECHANISM

In order to obtain the desired sensitivity in a McLeod gage of the aforementioned dimensions, it is necessary to measure the differential heights of the mercury columns (h in fig. 18) correct to 0.001 inch. Previous experience with the precision U-tube manometer (ref. 10) had shown that this could be accomplished satisfactorily by the use of suitable optical elements traveling on lead screws. The proper combination of threads and gears results in the appearance on a Veeder counter of the displacement of the optic along the lead screw, with a least count of 0.001 inch.

Special features of the McLeod gage reading mechanism are:

(1) Arrangement for measuring h in a carefully vertical orientation. Leveling screws are provided on the gage chassis, so that the lead screw can be oriented vertically before operation of the gage.

(2) A fine adjustment for the zeroing of the Veeder counter when the two optics have been determined to lie on a horizontal line. After the lead screw is made vertical, a U-tube open on both ends and about the same size as the McLeod capillaries is partially filled with mercury and set in place of the capillaries. When the meniscus in one leg of this tube is brought under the crosshair of the reference optic, the crosshair of the traveling optic can be set upon the meniscus in the other leg, using an adjusting nut by which the optic is attached to the lead screw. Just previous to this final adjustment the Veeder counter is set and left at zero, so that unless the adjusting nut works loose, or the lead screw gets out of its vertical orientation, the counter will always read zero when the traveling optic is horizontally opposite to the reference optic.

(3) Provision for the accurate placement of this horizontal reference line at $h = 0$ in coincidence with the top of the closed capillary. The lead screw and optics are mounted on a subchassis which can be raised or lowered on the basic chassis and locked in position by means of screws bearing against the top and bottom surfaces of the subchassis. The two chassis are clamped and keyed together, to provide rigidity in all horizontal directions.

The optical apparatus used in forming the images of the meniscuses is essentially identical to that employed on the precision U-tube manometer. It was found helpful in reducing refraction from the capillary walls to collimate the light from the source to a beam whose diameter matched the inside diameter of the capillary. The images obtained are quite large and clear, and the motion produced by a change in counter reading of 0.001 inch is easily detected. It is evident that, for the image to remain unchanged for all values of h, the closed capillary must be strictly parallel to the lead screw. If this does not result directly from a careful job of glassblowing, it can be obtained by shimming up the reservoir.

OPERATION OF GAGE

Besides the above-mentioned precautions in assembly and alinement of the gage and reading mechanism, special attention was given, during the operation of the gage, to the following items:

(1) A very slow and careful raising of the mercury to the seal-off point, to preserve the pressure equilibrium in the gage.

(2) A similarly cautious approach to the proper position of the mercury level in the reference capillary, aided by the use of the bellows on the reservoir. Contrary to expectations based on the performance of a previous McLeod gage of this size, it was found necessary to jar the gage at this point to free the mercury columns from some extraneous drag. Thus in the initial model of the gage, which was used during the impact-tube experiments, the final adjustment of the mercury level had to be made with a skillful combination of jarring and adjustment of the bellows.

CALIBRATION OF GAGE

The calibration formula for the gage was of the square-law form appropriate to this type of McLeod gage, modified by two correction terms, one to account for the finite volume of the closed capillary and the other, for the finite height of the mercury meniscuses. On the basis of conventional-type measurements of the capillary cross-sectional area and the compression volume, and a fairly crude estimate of a meniscus correction, the calibration formula was

$$p = 6.516h^2\left(1 + \frac{0.008}{h}\right)(1 + 0.0026h)$$

where h is to be measured in inches and p comes out in microns of mercury. The estimated probable error in this formula was 0.3 percent, but some fairly gross error in one of the measurements was suspected, after a program of comparison of the gage with the precision U-tube manometer. As was mentioned previously, the density of the manometer oil was very carefully determined, and when the manometer readings and McLeod readings were converted to absolute pressure units by use of the densities of oil and mercury, respectively, the McLeod pressures were, on an average, 1.4 percent higher. This problem, however, is not relevant to the present experimental program, since precise absolute calibration of the gage is of secondary importance in this context (affecting only Re, not C_μ or $p_i/p_{i(ideal)}$). For future use, the capillaries of the gage have recently been replaced with new ones of a superior internal finish and extraordinary uniformity of bore, and the entire calibration procedure has been repeated, using much superior measuring instruments and techniques. Although a full program of comparison of the recalibrated McLeod gage and the U-tube manometer has not been performed, preliminary data indicate much improved agreement between the two. At the same time the new capillaries appear to have reduced the problem of the sticking of the mercury in the capillaries to a relatively minor one.

ADVANTAGES AND DISADVANTAGES OF NEW GAGE

In discussing the relative merits of the new gage, the following items may be listed as definite improvements over its most recent predecessors.

(1) The optical system: Regardless of questions of accuracy, the present optical system is much easier on the eyes of the observer.

(2) The lead screw and counter: Inherently, the lead-screw and counter arrangement is more precise than an etched or scratched scale, and the counter virtually eliminated accidental reading errors.

(3) The metal reservoir: The metal reservoir reduces breakage worries, provides a rigid, flat-bottomed base for the gage, and has an economical shape allowing the use of long capillaries on a gage where the mercury is raised by atmospheric pressure alone.

(4) The longer capillaries: The longer capillaries have given the new gage a valuable increase in range, without sacrificing sensitivity or aggravating surface tension troubles.

On the other hand, the following disadvantages have appeared.

(1) Difficulty in cleaning the metal reservoir: The stainless steel has appeared quite satisfactory from a viewpoint of cleanliness and nonpollution of the mercury. The Kovar joints, on the contrary, do form amalgams if the mercury is accidentally splashed against them. The reservoir has proved somewhat difficult to clean and dry and has the disadvantage of being nontransparent, so that dirty spots cannot be seen.

(2) Sticking of mercury in the capillaries: The sticking of mercury in the capillaries seems to have been essentially overcome with the installation of the new capillaries. Even so, frequent and scrupulous cleanings of the gage and the mercury will probably be needed to insure a satisfactory condition.

(3) Handcrank operation of the lead screw: The driving of the lead screw by a handcrank is tiring to the operator, and motor drive for large level changes is recommended.

SUCCESS OF GAGE IN IMPACT-PRESSURE EXPERIMENTS

A final measure of the success of the gage in the present application is given by the data. A substantial reduction of scatter was achieved in comparison with the data of reference 2. Part of this was undoubtedly due to the more stable performance of the no. 3 wind tunnel (as compared with the no. 2 tunnel used for the work of ref. 2), but much appears to be due to the new gage. The chief disadvantage of the gage for the impact-pressure tests is the inherently large volume, which aggravates greatly the time-response problem of the apparatus.

APPENDIX C

ROTARY PROBE SELECTOR

GENERAL DESCRIPTION

The rotary probe selector consists essentially of a manifold in the shape of an octagonal disk, a driving and locating mechanism which rotates the manifold so that each of its eight faces comes in turn into a precisely fixed position, and a system of vacuum seals which provide a leak-proof channel between the manifold face which is "in position" and the pressure line to the manometers. The selector is mounted on the wind-tunnel traversing mechanism, so that three-directional translation, as well as rotation, of the device can be controlled remotely from the main console of the wind tunnel. Figure 19 shows the selector, outfitted with eight probes, in position with respect to nozzle 6. A complete set of assembly and detail drawings is on file at the Fluid Mechanics Laboratory, under the numbers L.P. 61-6-0 to 61-6-12.

CONSTRUCTION

The design of the mechanism makes special use of the principle of the Geneva movement for transmission of the motion from the electric-motor output to the rotating manifold and for the accurate positioning of the manifold (see fig. 20). The particular design of Geneva movement was chosen to provide an intermittent rotational output in response to the steady turning of the input shaft. To utilize this feature a cam is mounted beside the Geneva pinwheel on the input shaft to provide motion of a piston which makes an O-ring vacuum seal against the manifold (see fig. 21). The cam is set so that the seating and retracting of the sealing piston take place during the stationary periods in the Geneva movement output, thus avoiding undesirable friction between the O-ring and the manifold, with possible damage to the O-ring. A microswitch activated by another cam on the input shaft stops the electric motor after the manifold has reached an operating position and the sealing piston has been seated. Special precautions were exercised in choice of gears, bearings, and other parts to minimize mechanical backlash and looseness between the Geneva output wheel and the manifold. Vacuum seals throughout were of conventional O-ring types.

OPERATING CYCLE

To turn the selector from one position to the next:

(a) A manual switch at the wind-tunnel console shorts out the microswitch, starting the motor in either the clockwise or counterclockwise direction, as dictated by a selecting switch.

(b) The Geneva pinwheel turns through its first 45°, while the slotted wheel stands still and the two cams activate the opening of the microswitch and the retracting of the sealing piston.

(c) The pinwheel continues through its next 90°, during which it engages the slotted wheel and turns it 90°. The angular output of the slotted wheel is reduced by a factor of 2 through special antibacklash gears, so that the manifold executes just one-eighth of a turn, bringing its next face into position. The locking surfaces of the pin and slotted wheels begin engagement.

(d) The pinwheel completes its half revolution while the final precise positioning of the slotted wheel is accomplished by the mating of the locking surfaces, and the two cams activate the seating of the sealing piston and the closing of the microswitch, stopping the motor.

CONCLUSION

Both the positioning and sealing features of the selector have proved entirely satisfactory in use during the impact-pressure experiments, and the device as a whole has been a valuable addition to the wind-tunnel instrumentation.

APPENDIX D

TESTS IN AN INDEPENDENTLY CALIBRATED SUPERSONIC AIR STREAM

INTRODUCTION

A new nozzle for use in the no. 3 wind tunnel has recently been designed and upon experimental evaluation has proved quite superior to the nozzles employed for the impact-pressure experiments. In particular, the new nozzle has been shown to produce an isentropic acceleration from the stagnation chamber to the test section, thus allowing a calibration of its flow independent of either static or impact probes. This is achieved satisfactorily by measurement of the stagnation-chamber pressure and temperature and the pressure at the nozzle wall near the exit plane. Constancy of static pressure across the exit section of the nozzle is assumed when the wall static and test-chamber pressures are balanced. This new nozzle is designated nozzle 8 and is described in reference 18, from which the following pertinent performance data are taken:

Flow rate, lb/hr	M	p_s, microns	Re (L = 1 in.)	Diameter of isentropic core, in.
5.2	3.70	50	920	1.3
10.3	3.89	75	1,600	1.9
14	3.98	90	2,100	2.3
20	4.06	112	2,800	2.4
26	4.13	134	3,600	2.7

(Stagnation temperature = Room temperature ≈ 535° R)

The radial distribution of impact pressures is shown for the four lowest flow rates in figure 22.

TEST PROCEDURE AND DATA REDUCTION

The static pressures listed above were sensed by a 1/16-inch-diameter wall tap located 2 inches upstream from the nozzle exit (at which position the velocity at the isentropic core boundary was within 0.2 percent of its exit-plane value) and measured with the precision McLeod gage. The measurement was taken when the jet was free of models and when the test-chamber and wall-tap pressures were accurately balanced (within

3/4 percent at the worst). It should be remarked that the insertion of a probe destroyed this balance somewhat by lowering the test-chamber pressure a few percent. The latter effect had been remarked in previous tests but was not investigated in detail. It is assumed that the small unbalance so produced will have a negligible effect on the flow properties close to the nozzle axis at the exit plane, where the impact pressures were taken.

The Mach number was computed from the ratio of the measured static pressure and stagnation-chamber pressure, with the assumption of isentropic flow along the nozzle axis and of constant static pressure across the nozzle cross section at which the wall tap was located. The ideal impact pressure was computed from the static pressure and the Mach number by the Rayleigh pitot-tube formula.

Four type B probes and four type C probes were mounted at once on the rotary probe selector and tested at two positions in the nozzle exit plane, first on the nozzle axis and second at 0.300 inch above the axis. Impact pressures (and the stagnation-chamber pressure) were measured on the n-butyl phthalate U-tube manometer as in the tests in the previous nozzles.

RESULTS

Figure 23 shows the results of these tests at the off-axis position. The data on the axis are entirely similar, pressures being displaced by an amount which is in accord with the results shown in figure 22. In figure 23 extrapolation curves have been drawn in a fashion similar to those shown in figure 6. The intercepts arrived at by these curves fall within about 1 percent of the $p_{i(ideal)}$ values obtained by the isentropic-flow assumption. The discrepancies encountered were not systematic and would depend in magnitude on the location of the test point in the nozzle flow.

Unfortunately the Reynolds numbers per inch characterizing nozzle 8 are so high that it was impossible to obtain large viscous effects on even the smallest impact probes which could be used. Consequently, the present experiments, in which the probe readings, the extrapolated $p_{i(ideal)}$, and the independently calculated $p_{i(ideal)}$ were all in agreement within a very few percent, do not give a direct validation of the extrapolation procedure in the cases where its application is most suspect (i.e., at the lowest extreme of the Reynolds number range). Neither was the flow in the new nozzle so uniform as to permit a very close check (<1 percent) on the accuracy of extrapolation. On the other hand, it is encouraging to see from the new experiments that the extrapolation procedure has not yielded results which are definitely wrong.

An important byproduct of the calibration of nozzle 8 was information concerning the accuracy of static pressures derived from the conical static probe (see discussion of this probe in appendix A). This value of the static pressure was of the order of 20 percent higher than the true static pressure measured by the wall tap. The Mach number value deduced by use of the cone probe was correspondingly about 10 percent too low. These errors are serious and indicate that correspondingly serious errors exist in the Mach numbers and static pressures listed for nozzles 2A, 3, and 6. Fortunately, for the present purpose, these errors are to a large extent mutually canceled in the calculation of C_μ and Re. (Thus, for nozzle 8, the C_μ value is entirely unchanged and the Reynolds number affected by only about 3 percent by the errors quoted above.)

A qualitative observation of some significance may be made concerning Mach number effects on the viscous correction to impact pressures in view of the data for nozzle 8. First, the existence of "negative" as well as of "positive" viscous effects is very pronounced in these data, and, secondly, it may be remarked that at a Mach number of 4.06 even the highest Reynolds number reached (about 850) is not sufficient to bring about a better than 1 percent agreement between type B and type C probes. Furthermore, if the extrapolations made in figure 23 are used to give $p_{i(ideal)}$ and the data are processed to yield a plot of C_{μ_2} against $1/Re_2$, these new data lie on a direct continuation of the Mach number trend inferred from the data in the main body of the report.

CONCLUSIONS

The preliminary results of tests in a new supersonic nozzle indicated the following conclusions:

(1) The process of extrapolation yields values of the ideal impact pressure which are in agreement with values determined independently in a nozzle producing isentropic flow, the agreement being as close as could be expected under the present conditions of flow uniformity and experimental accuracy.

(2) The static pressure deduced from a conical static probe in this nozzle flow is seriously in error (being about 20 percent too high), but this error has relatively little effect on the calculated values of C_μ and Reynolds number (<3 percent).

(3) The general trend of Mach number effects on impact-pressure viscous corrections noted in nozzles 2A, 3, and 6 is continued in this

nozzle up to a Mach number of 4.06. In particular, the negative viscous effects detected under certain conditions in the other nozzles were very prominent in the new nozzle and are definitely an effect of increasing Mach number rather than of flow nonuniformities.

REFERENCES

1. Kane, E. D., and Maslach, G. J.: Impact-Pressure Interpretation in a Rarefied Gas at Supersonic Speeds. NACA TN 2210, 1950.

2. Kane, E. D., and Schaaf, S. A.: Viscous Effects on Impact Probes in a Subsonic Rarefied Gas Flow. Rep. No. HE-150-82, Contract NAw-5754, NACA and Univ. of Calif., Mar. 9, 1951.

3. Chambré, P. L., and Smith, H. R.: The Impact Tube in a Viscous Compressible Gas. Rep. No. HE-150-63, Contract No. N7-ONR-295-Task 3, Office of Naval Res. and Eng. Res. Projects, Univ. of Calif., Aug. 29, 1949. (Also, Heat Transfer and Fluid Mechanics Inst., A.S.M.E., 1949, pp. 271-278.)

4. Chambré, P. L.: The Theory of the Impact Tube in a Viscous Compressible Gas. Rep. No. HE-150-50, Contract No. N7-ONR-295-Task 3, Office of Naval Res. and Eng. Res. Projects, Univ. of Calif., Nov. 1, 1948.

5. Lin, T. C., and Schaaf, S. A.: Effect of Slip on Flow Near a Stagnation Point and in a Boundary Layer. NACA TN 2568, 1951.

6. Ipsen, D. C.: Viscosity Correction to Impact Pressure on Prolate Spheroid. Rep. No. HE-150-89, Contract N7-ONR-295-Task 3, Office of Naval Res., Air Res. and Dev. Command, and Inst. Eng. Res., Univ. of Calif., Mar. 12, 1952.

7. Kane, E. D.: Drag Forces on Spheres in Low Density Supersonic Gas Flows. Rep. No. HE-150-65, Contract No. N7-ONR-295-Task 3, Office of Naval Res. and Eng. Res. Projects, Univ. of Calif., Feb. 15, 1950. (Also, Sphere Drag Data at Supersonic Speeds and Low Reynolds Numbers. Jour. Aero. Sci., vol. 18, no. 4, Apr. 1951, pp. 259-270.)

8. Emerson, D. E., and Schaaf, S. A.: Performance of a Supersonic Nozzle in the Rarefied Gas Dynamics Regime. Rep. No. HE-150-72, Contract No. N7-ONR-295-Task 3, Office of Naval Res. and Eng. Res. Projects, Univ. of Calif., Aug. 1950.

9. Marks, Lionel S., ed.: Mechanical Engineers' Handbook. Fourth ed., McGraw-Hill Book Co., Inc., 1941, p. 2100.

10. Maslach, G. J.: A Precision Manometer for Low Pressures. Rep. No. HE-150-75, Contract No. N7-onr-295-Task 3, Office of Naval Res. and Inst. Eng. Res., Univ. of Calif., Oct. 27, 1950.

11. Homann, Fritz: Der Einfluss grosser Zähigkeit bei der Strömung um den Zylinder und um die Kugel. Z.a.M.M., Bd. 16, Heft 3, June 1936, pp. 153-164. (Available in English translation as NACA TM 1334.)

12. Barker, Muriel: On the Use of Very Small Pitot-Tubes for Measuring Wind Velocity. Proc. Roy. Soc. (London), ser. A, vol. 101, 1922, pp. 435-445.

13. Staff of the Computing Section (under the direction of Zdenek Kopal): Tables of Supersonic Flow Around Cones. Tech. Rep. No. 1, Center of Analysis, M.I.T., 1947.

14. Morey, F. C.: Dry Air. NBS-NACA Tables of Thermal Properties of Gases, Table 2.39, Dec. 1950.

15. Emmons, Howard W.: Gas Dynamics Tables for Air. Dover Publications, 1947.

16. Hodgman, Charles D., ed.: Handbook of Chemistry and Physics. Twenty-first ed., Chem. Rubber Pub. Co. (Cleveland), 1936, p. 9.

17. Lin, T. C., Schaaf, S. A., and Sherman, F. S.: Boundary Layer Effect on the Surface Pressure of an Infinite Cone in Supersonic Flow. Rep. No. HE-150-80, Contract NAw-6004, NACA and Univ. of Calif., Mar. 5, 1951.

18. Owen, J. M., and Sherman, F. S.: Design and Testing of a Mach 4 Axially Symmetric Nozzle for Rarefied Gas Flows. Rep. No. HE-150-104, Contract No. N7-onr-295, Office of Naval Res., Office of Sci. Res., and Inst. Eng. Res., Univ. of Calif., July 23, 1952.

19. Merriam, Kenneth G., and Spaulding, Ellis R.: Comparative Tests of Pitot-Static Tubes. NACA TN 546, 1935.

TABLE I.- SUMMARY OF DATA AND RESULTS FOR SUBSONIC AIR STREAMS

Flow rate, lb/hr	Probe type	T_o, °R	d, in.	p_i, μ Hg	p_s, μ Hg	p_o, μ Hg (a)	p_i/p_s	$\overline{\left(\frac{p_o}{p_s}\right)}$	M	C_μ	Re	1/Re
50	B	543	1.500	3,276	3,252		1.007	1.007	0.102	0	365	0.0027
			1.500	3,273	3,250	3,273	1.007			0	365	.0027
			1.000	3,275	3,252		1.007			0	243	.0041
			1.000	3,273	3,248		1.008			.137	243	.0041
			.500	3,278	3,254	3,277	1.007			0	122	.0082
			.500	3,274	3,250		1.007			0	122	.0082
			.150	3,281	3,252	3,275	1.009			.285	36.5	.0274
			.150	3,277	3,247	3,270	1.009			.285	36.4	.0275
50	C	543	1.500	3,274	3,250	3,275	1.007	1.007	.102	0	364	.0028
			1.500	3,269	3,246	3,269	1.007			0	364	.0028
			1.000	3,277	3,254	3,277	1.007			0	243	.0041
			1.000	3,273	3,250		1.007			0	243	.0041
			.500	3,275	3,252		1.007			0	122	.0082
			.500	3,272	3,248		1.007			0	121	.0082
			.150	3,277	3,254		1.007			0	36.5	.0274
			.150	3,275	3,250		1.008			.137	36.5	.0274
50	B	544	1.500	1,605	1,554		1.033	1.032	.212	.032	365	.0027
			1.500	1,603	1,552		1.033			.032	364	.0028
			1.000	1,605	1,554		1.033			.032	243	.0041
			1.000	1,604	1,552		1.034			.064	243	.0041
			.500	1,607	1,554	1,603	1.034			.064	122	.0082
			.500	1,606	1,553		1.034			.064	122	.0082
			.150	1,619	1,555		1.041			.286	36.5	.0274
			.150	1,617	1,552	1,603	1.042			.318	36.4	.0275
50	C	544	1.500	1,605	1,554		1.033	1.032	.212	.032	365	.0027
			1.500	1,603	1,552		1.033			.032	364	.0028
			1.000	1,605	1,554		1.033			.032	243	.0041
			1.000	1,603	1,553		1.032			0	243	.0041
			.500	1,603	1,554		1.032			0	122	.0082
			.500	1,603	1,552		1.033			.032	121	.0082
			.150	1,608	1,556	1,605	1.033			.032	36.5	.0274
			.150	1,607	1,554	1,602	1.034			.064	36.5	.0274
50	B	538	1.500	981	895		1.096	1.094	.360	.022	371	.0027
			1.500	980	895		1.095			.011	371	.0027
			1.000	981	895		1.096			.022	248	.0040
			1.000	980	895		1.095			.011	248	.0040
			.500	985	895		1.101			.077	124	.0081
			.500	985	895		1.101			.077	124	.0081
			.150	1,002	895	979	1.120			.287	37.1	.0269
			.150	1,001	895	978	1.118			.265	37.1	.0269
50	C	538	1.500	982	896	981	1.096	1.094	.360	.022	372	.0027
			1.500	981	895	979	1.096			.022	371	.0027
			1.000	980	895		1.095			.011	248	.0040
			1.000	979	895		1.094			0	248	.0040
			.500	979	894		1.095			.011	124	.0081
			.500	978	894		1.094			0	124	.0081
			.150	984	896	980	1.098			.044	37.1	.0269
			.150	985	896	979	1.099			.055	37.1	.0269
36	B	540	1.500	2,387	2,370		1.007	1.007	.098	0	257	.0039
			1.500	2,385	2,368		1.007			0	257	.0039
			1.000	2,387	2,370		1.007			0	171	.0058
			1.000	2,385	2,368		1.007			0	171	.0058
			.500	2,390	2,372	2,387	1.008			.149	85.8	.0117
			.500	2,387	2,368		1.008			.149	85.6	.0117
			.150	2,392	2,370	2,385	1.009			.298	25.7	.0389
			.150	2,390	2,368	2,383	1.009			.298	25.7	.0389
36	C	540	1.500	2,386	2,369	2,386	1.007	1.007	.098	0	257	.0039
			1.500	2,383	2,367	2,384	1.007			0	257	.0039
			1.000	2,388	2,372		1.007			0	171	.0058
			1.000	2,385	2,368		1.007			0	171	.0058
			.500	2,387	2,370		1.007			0	85.7	.0117
			.500	2,385	2,368		1.007			0	85.7	.0117
			.150	2,389	2,371		1.008			.149	25.7	.0389

[a] p_o was measured only at those points where it is listed in the table.

TABLE I.- SUMMARY OF DATA AND RESULTS FOR SUBSONIC AIR STREAMS - Continued

Flow rate, lb/hr	Probe type	T_o, °R	d, in.	p_i, μ Hg	p_s, μ Hg	p_o, μ Hg (a)	p_i/p_s	$\left(\frac{p_o}{p_s}\right)$	M	C_μ	Re	1/Re
36	B	542	1.500	1,180	1,143		1.032	1.032	0.212	0	270	0.0037
			1.500	1,179	1,141		1.033			.032	270	.0037
			1.000	1,180	1,143		1.032			0	180	.0056
			1.000	1,179	1,140		1.034			.064	180	.0056
			.500	1,183	1,144		1.034			.064	90.0	.0111
			.500	1,182	1,142		1.035			.095	90.0	.0111
			.150	1,194	1,144	1,179	1.044			.381	27.0	.0370
			.150	1,192	1,142	1,179	1.044			.381	27.0	.0370
36	C	542	1.500	1,179	1,142	1,178	1.032	1.032	.212	0	270	.0037
			1.500	1,178	1,140	1,177	1.033			.032	270	.0037
			1.000	1,180	1,144		1.032			0	180	.0056
			1.000	1,178	1,142		1.032			0	180	.0056
			.500	1,180	1,144		1.032			0	90.0	.0111
			.500	1,179	1,142		1.032			0	90.0	.0111
			.150	1,184	1,145		1.034			.064	27.0	.0370
			.150	1,182	1,144		1.033			.032	27.0	.0370
26	B	543	1.500	1,803	1,790		1.007	1.006	.097	.152	192	.0052
			1.500	1,799	1,786		1.007			.152	191	.0052
			1.000	1,801	1,788		1.007			.152	128	.0078
			1.000	1,799	1,786		1.007			.152	128	.0078
			.500	1,804	1,790	1,802	1.008			.303	63.8	.0157
			.500	1,801	1,786		1.008			.303	63.8	.0157
			.150	1,805	1,787	1,799	1.010			.607	19.1	.0523
			.150	1,804	1,786	1,797	1.010			.607	19.1	.0523
26	C	543	1.500	1,799	1,787	1,799	1.007	1.006	.097	.152	191	.0052
			1.500	1,799	1,786	1,797	1.007			.152	191	.0052
			1.000	1,802	1,790		1.007			.152	128	.0078
			1.000	1,799	1,787		1.007			.152	128	.0078
			.500	1,800	1,788		1.007			.152	63.8	.0157
			.500	1,797	1,786		1.006			0	63.8	.0157
			.150	1,804	1,790		1.008			.303	19.2	.0522
			.150	1,801	1,786		1.008			.303	19.1	.0523
26	B	543	1.500	905	878		1.031	1.028	.199	.108	194	.0051
			1.500	903	878		1.029			.036	194	.0051
			1.000	905	880		1.028			0	130	.0077
			1.000	904	878		1.030			.072	130	.0077
			.500	908	880	905	1.032			.144	64.8	.0154
			.500	908	878		1.034			.216	64.8	.0154
			.150	918	880	903	1.043			.541	19.5	.0513
			.150	917	878		1.044			.577	19.4	.0514
26	C	543	1.500	903	878		1.029	1.028	.199	.036	194	.0051
			1.500	903	877	903	1.030			.072	194	.0051
			1.000	905	880		1.028			0	130	.0077
			1.000	904	878		1.030			.072	130	.0077
			.500	905	880		1.028			0	64.8	.0154
			.500	903	878		1.029			.036	64.8	.0154
			.150	910	880		1.034			.216	19.5	.0513
			.150	908	879		1.033			.180	19.5	.0513
36	B	530	1.500	747.5	681.5	744.7	1.097	1.092	.357	.056	286	.0035
			1.000	747.8	680.6		1.099			.078	191	.0052
			.500	751.3	683.5		1.099			.078	95.5	.0105
			.300	755.2	682.6		1.106			.157	57.3	.0175
36	C	530	1.500	745.3	681.5	744.7	1.094	1.092	.357	.022	286	.0035
			1.000	746.3	682.6		1.093			.011	191	.0052
			.500	745.7	682.7		1.092			0	95.5	.0105
			.300	747.1	680.6		1.098			.067	57.3	.0175
26	B	537	1.500	534.4	482.2	533.8	1.108	1.103	.376	.051	212	.0047
			1.000	537.5	483.9		1.111			.081	141	.0071
			.500	540.1	484.7		1.114			.111	70.5	.0142
			.300	545.1	484.3		1.126			.233	42.3	.0236
26	C	537	1.500	535.1	484.3	533.8	1.105	1.103	.376	.020	212	.0047
			1.000	534.4	484.8		1.102			-.010	141	.0071
			.500	534.5	484.9		1.102			-.010	70.5	.0142
			.300	536.1	483.8		1.108			.051	42.3	.0236

[a] p_o was measured only at those points where it is listed in the table.

NACA

TABLE I.- SUMMARY OF DATA AND RESULTS FOR SUBSONIC AIR STREAMS - Concluded

Flow rate, lb/hr	Probe type	T_0, °R	d, in.	p_i, μ Hg	p_s, μ Hg	p_0, μ Hg (a)	p_i/p_s	$\left(\frac{p_0}{p_s}\right)$	M	C_μ	Re	1/Re
10.3	B	538	1.500	392.6	380.2	390.7	1.033	1.030	0.206	0.101	88.2	0.0113
			1.000	392.4	379.1		1.035			.169	58.8	.0170
			.500	395.2	379.9		1.040			.337	29.4	.0340
			.300	398.2	379.8		1.048			.607	17.6	.0568
10.3	C	538	1.500	390.9	378.7	390.7	1.032	1.030	.206	.067	88.2	.0113
			1.000	391.3	379.2		1.032			.067	58.8	.0170
			.500	391.6	379.4		1.032			.067	29.4	.0340
			.300	394.6	378.1		1.044			.471	17.6	.0568
36	B	538	1.500	510.6	399.6	506.3	1.278	1.265	.589	.054	286	.0035
			1.000	510.5	398.9		1.280			.062	191	.0052
			.500	516.2	399.9		1.291			.107	95.5	.0105
			.300	524.9	399.9		1.313			.197	57.3	.0175
36	C	538	1.500	513.2	402.7	506.3	1.274	1.265	.589	.037	286	.0035
			1.000	509.1	400.4		1.271			.025	191	.0052
			.500	508.5	400.8		1.269			.016	95.5	.0105
			.300	510.9	401.4		1.273			.034	57.3	.0175
26	B	532	1.500	357.0	266.8	352.3	1.338	1.322	.644	.055	216	.0046
			1.000	356.9	265.7		1.343			.072	144	.0069
			.500	363.2	266.2		1.364			.144	72.0	.0139
			.300	370.8	264.9		1.400			.269	43.2	.0231
26	C	532	1.500	358.0	270.9	352.3	1.322	1.322	.644	0	216	.0046
			1.000	353.4	266.2		1.328			.021	144	.0069
			.500	352.0	265.4		1.326			.014	72.0	.0139
			.300	354.8	266.2		1.333			.038	43.2	.0231
10.3	B	537	1.500	215.3	190.6	212.5	1.130	1.117	.401	.115	89.0	.0112
			1.000	215.6	190.0		1.135			.160	59.3	.0169
			.500	220.2	189.2		1.164			.417	29.6	.0338
			.300	226.5	191.0		1.186			.613	17.8	.0562
10.3	C	537	1.500	213.4	190.3	212.5	1.121	1.117	.401	.035	89.0	.0112
			1.000	212.9	191.0		1.115			-.018	59.3	.0169
			.500	214.7	190.0		1.130			.012	29.6	.0338
			.300	217.1	189.5		1.146			.257	17.8	.0562
10.3	B	538	1.500	152.6	111.4	148.0	1.370	1.349	.668	.067	91.4	.0109
			1.000	154.8	109.9		1.409			.193	60.9	.0164
			.500	160.8	108.9		1.477			.410	30.4	.0329
			.300	167.9	108.8		1.543			.621	18.3	.0546
10.3	C	538	1.500	149.0	111.5	148.0	1.336	1.349	.668	-.042	91.4	.0109
			1.000	147.8	110.0		1.344			-.016	60.9	.0164
			.500	149.6	108.6		1.378			.093	30.4	.0329
			.300	154.6	108.8		1.421			.230	18.3	.0546
2.3	B	536	1.500	131.5	128.0	130.5	1.027	1.019	.164	.430	23.6	.0424
			1.000	132.4	128.2		1.033			.731	15.7	.0637
			.500	133.9	128.0		1.046			1.450	7.8	.128
			.300	135.6	127.8		1.061			2.256	4.7	.213
2.3	C	536	1.500	131.5	128.1	130.5	1.027	1.019	.164	.430	23.6	.0424
			1.000	131.4	128.3		1.024			.269	15.7	.0637
			.500	132.1	128.1		1.031			.644	7.8	.128
			.300	133.5	128.0		1.043			1.289	4.7	.213
2.3	B	536	1.500	66.24	58.49	63.46	1.133	1.082	.338	.639	23.0	.0435
			1.000	67.32	58.63		1.148			.827	15.3	.0654
			.500	70.53	58.44		1.207			1.566	7.6	.1318
			.300	73.01	58.55		1.247			2.067	4.6	.2175
2.3	C	536	1.500	64.60	58.98	63.46	1.095	1.082	.338	.163	23.0	.0435
			1.000	65.33	58.79		1.111			.363	15.3	.0654
			.500	67.20	58.59		1.147			.814	7.6	.1318
			.300	70.08	58.55		1.197			1.441	4.6	.2175
2.3	B	531	1.500	47.43	36.55	42.70	1.298	1.195	.512	.561	22.2	.0450
			1.000	48.67	35.89		1.356			.879	14.8	.0676
			.500	52.31	35.40		1.478			1.543	7.4	.1352
			.300	56.10	35.99		1.559			1.984	4.4	.2250
2.3	C	531	1.500	44.75	35.81	42.70	1.250	1.195	.512	.300	22.2	.0450
			1.000	45.30	35.78		1.266			.387	14.8	.0676
			.500	48.26	35.19		1.371			.960	7.4	.1352
			.300	51.59	35.13		1.469			1.494	4.4	.2250

[a] p_0 was measured only at those points where it is listed in the table.

NACA

TABLE II.- SUMMARY OF DATA AND RESULTS FOR SUPERSONIC AIR STREAMS

[See appendix A for calculation methods]

Flow rate, lb/hr	Probe type	T_o, °R	p_2, μ Hg	d, in.	p_i, μ Hg	$p_{i(ideal)}$, μ Hg	M	Re	$\frac{p_i}{p_{i(ideal)}}$	C_{μ_2}	$1/Re_2$
Nozzle 6											
30	B	531	244.8	1.000	1,284.5	1,285.1	2.02	757	1.000	-0.003	0.0021
	B			.500	1,283.1			378	.998	-.008	.0042
	B			.300	1,283.6			227	.999	-.005	.0069
	B			.150	1,295.5			114	1.008	.043	.0139
	C			1.000	1,283.6			757	.999	-.005	.0021
	C			.500	1,285.5			378	1.000	.016	.0042
	C			.150	1,279.1			114	.995	-.024	.0139
26	B	536	216.9	1.000	1,124.8	1,125.5	2.01	654	.999	-.003	.0024
	B			.500	1,125.3			327	1.000	-.001	.0048
	B			.300	1,124.4			196	.999	-.005	.0079
	B			.150	1,140.3			98.1	1.013	.070	.0158
	C			1.000	1,121.9			654	.997	-.016	.0024
	C			.500	1,125.3			327	1.000	-.001	.0048
	C			.150	1,119.4			98.1	.995	-.029	.0158
20	B	536	174.6	1.000	881.1	881.7	1.98	513	.999	-.003	.0030
	B			.500	882.6			257	1.001	.005	.0060
	B			.300	884.6			154	1.003	.018	.0100
	B			.150	904.5			77.0	1.026	.137	.0200
	C			1.000	878.6			513	.996	-.018	.0030
	C			.500	882.1			257	1.000	.003	.0060
	C			.150	875.6			77.0	.993	-.037	.0200
15.5	B	537	145.3	1.000	715.9	715.6	1.95	409	1.000	.003	.0037
	B			.500	717.9			205	1.003	.018	.0074
	B			.300	721.9			123	1.009	.047	.0123
	B			.150	745.8			61.4	1.042	.220	.0246
	C			1.000	712.4			409	.996	-.023	.0037
	C			.500	715.9			205	1.000	.003	.0074
	C			.150	710.4			61.4	.993	-.039	.0246
30	B	532	247.8	1.000	1,295.5	1,295.5	2.02	762	1.000	0	.0021
	B			.500	1,295.5			381	1.000	0	.0041
	B			.300	1,296.5			229	1.001	.005	.0068
	B			.150	1,307.4			114	1.009	.049	.0137
	C			1.000	1,295.5			762	1.000	0	.0021
	C			.500	1,296.5			381	1.001	.005	.0041
	C			.150	1,289.5			114	.995	-.024	.0137
20	B	532	175.1	1.000	883.6	883.7	1.98	520	1.000	-.001	.0030
	B			.500	884.6			260	1.001	.005	.0060
	B			.300	887.5			156	1.004	.024	.0099
	B			.150	905.4			77.9	1.025	.132	.0199
	C			1.000	881.6			520	.998	-.013	.0030
	C			.500	883.6			260	1.000	-.001	.0060
	C			.150	877.6			77.9	.993	-.037	.0199
10.3	B	528	110.4	1.000	501.5	501.4	1.86	288	1.000	.001	.0051
	B			.500	503.5			144	1.004	.021	.0102
	B			.300	509.9			86.5	1.017	.085	.0171
	B			.150	535.3			43.2	1.068	.339	.0342
	C			1.000	500.0			288	.997	-.014	.0051
	C			.500	500.0			144	.997	-.014	.0102
	C			.150	497.5			43.2	.992	-.039	.0342

NACA

TABLE II.- SUMMARY OF DATA AND RESULTS FOR SUPERSONIC AIR STREAMS - Continued

Flow rate, lb/hr	Probe type	T_o, °R	p_2, μ Hg	d, in.	p_i, μ Hg	p_i(ideal), μ Hg	M	Re	$\frac{p_i}{p_i(\text{ideal})}$	C_{μ_2}	$1/Re_2$
Nozzle 6											
5.2	B	531	71.6	1.000	283.6	279.7	1.69	154	1.014	0.064	0.0089
	B			.500	287.6			77.2	1.028	.129	.0179
	B			.300	297.0			46.3	1.062	.182	.0298
	B			.150	325.4			23.2	1.163	.746	.0596
	C			1.000	279.6			154	1.000	-.002	.0089
	C			.500	278.1			77.2	.994	-.026	.0179
	C			.150	284.1			23.2	1.016	.072	.0596
30	B	532	247.3	1.000	1,290.0	1,290.5	2.02	760	1.000	-.002	.0021
	B			.500	1,288.5			380	.999	-.007	.0041
	B			.300	1,290.5			228	1.000	0	.0069
	B			.225	1,293.0			171	1.002	.011	.0092
	B			.150	1,299.5			114	1.007	.038	.0137
	C			.500	1,289.0			380	.999	-.006	.0041
	C			.150	1,283.6			114	.995	-.029	.0137
26	B	531	218.6	1.000	1,127.3	1,127.8	2.00	661	1.000	-.002	.0024
	B			.500	1,126.8			331	.999	-.005	.0047
	B			.300	1,129.3			198	1.001	.007	.0079
	B			.225	1,134.8			149	1.006	.033	.0105
	B			.150	1,144.2			99.2	1.014	.078	.0157
	C			.500	1,127.3			331	1.000	-.002	.0047
	C			.150	1,121.9			99.2	.995	-.028	.0157
20	B	533	177.1	1.000	880.6	881.1	1.96	511	.999	-.003	.0030
	B			.500	881.6			256	1.001	.003	.0060
	B			.300	886.0			153	1.006	.029	.0100
	B			.225	891.5			115	1.012	.062	.0133
	B			.150	903.5			76.6	1.025	.134	.0200
	C			.500	882.6			256	1.002	.009	.0060
	C			.150	873.6			76.6	.992	-.045	.0200
15.5	B	532	147.3	1.000	717.9	717.0	1.93	413	1.001	.007	.0037
	B			.500	718.4			207	1.002	.010	.0073
	B			.300	724.4			124	1.010	.054	.0122
	B			.225	730.3			93.0	1.018	.096	.0163
	B			.150	745.8			62.0	1.040	.209	.0244
10.3	B	534	109.4	1.000	501.5	498.3	1.86	282	1.006	.032	.0052
	B			.500	504.5			141	1.012	.062	.0104
	B			.300	510.9			84.7	1.025	.127	.0173
	B			.225	519.4			63.5	1.042	.212	.0231
	B			.150	536.8			42.3	1.077	.387	.0347
5.2	B	533	70.6	1.000	279.6	276.1	1.69	152	1.013	.058	.0091
	B			.500	285.6			75.7	1.034	.157	.0182
	B			.300	295.5			45.4	1.070	.321	.0303
	B			.225	305.0			34.1	1.105	.478	.0403
	B			.150	320.4			22.7	1.160	.732	.0605
30	C	537	245.1	.600	1,290.5	1,290.5	2.03	451	1.000	0	.0035
	C			.450	1,290.5			338	1.000	0	.0046
	C			.300	1,290.5			225	1.000	0	.0069
	C			.225	1,289.0			169	.999	-.006	.0092
	C			.150	1,284.5			113	.995	-.025	.0139
	C			.100	1,275.9			75.1	.989	-.062	.0208
26	C	540	218.5	.600	1,134.9	1,134.9	2.01	390	1.000	0	.0040
	C			.450	1,134.9			293	1.000	0	.0053
	C			.300	1,133.9			195	.999	-.005	.0079
	C			.225	1,131.9			146	.997	-.014	.0105
	C			.150	1,128.4			97.6	.994	-.031	.0158
	C			.100	1,124.4			65.1	.991	-.050	.0237

NACA

TABLE II.- SUMMARY OF DATA AND RESULTS FOR SUPERSONIC AIR STREAMS - Continued

Flow rate, lb/hr	Probe type	T_o, °R	p_2, μ Hg	d, in.	p_i, μ Hg	$p_{i(ideal)}$, μ Hg	M	Re	$\frac{p_i}{p_{i(ideal)}}$	C_{μ_2}	$1/Re_2$
					Nozzle 6						
20	C	541	174.8	0.600	882.1	882.2	1.98	301	1.000	-0.001	0.0051
	C			.450	882.1			226	1.000	-.001	.0067
	C			.300	881.6			150	.999	-.004	.0101
	C			.225	879.6			113	.997	-.016	.0135
	C			.150	876.1			75.2	.993	-.037	.0202
	C			.100	875.1			50.1	.992	-.043	.0304
15.5	C	542	143.7	.600	717.3	718.0	1.97	245	.999	-.005	.0062
	C			.450	717.3			183	.999	-.005	.0083
	C			.300	716.3			122	.998	-.013	.0124
	C			.225	713.8			91.7	.994	-.031	.0165
	C			.150	712.3			61.1	.992	-.042	.0248
	C			.100	713.8			40.8	.994	-.031	.0372
10.3	C	543	108.0	.600	501.8	502.2	1.88	168	.999	-.004	.0087
	C			.450	501.3			126	.998	-.009	.0116
	C			.300	498.8			83.8	.993	-.034	.0175
	C			.225	498.3			62.9	.992	-.039	.0233
	C			.150	498.3			41.9	.992	-.039	.0349
	C			.100	506.3			27.9	1.008	.041	.0533
5.2	C	543	66.3	.600	277.3	277.5	1.76	90.3	.999	-.003	.0155
	C			.450	276.3			67.7	.996	-.021	.0206
	C			.300	275.3			45.2	.992	-.038	.0309
	C			.225	276.3			33.9	.996	-.021	.0412
	C			.150	281.8			22.6	1.016	.074	.0619
	C			.100	297.4			15.1	1.072	.341	.0928
30	A	536	247.0	.600	1,289.4	1,285.5	2.01	447	1.003	.016	.0035
	A			.450	1,293.4			335	1.006	.033	.0046
	A			.300	1,292.4			223	1.005	.029	.0070
	A			.225	1,295.4			168	1.008	.042	.0093
	A			.150	1,300.3			112	1.012	.063	.0139
26	A	537	218.7	.600	1,132.3	1,126.0	2.00	391	1.006	.030	.0040
	A			.450	1,133.3			293	1.006	.035	.0053
	A			.300	1,135.3			196	1.008	.044	.0079
	A			.225	1,136.3			147	1.009	.049	.0106
	A			.150	1,143.3			97.7	1.015	.083	.0158
20	A	538	174.0	.600	884.8	879.0	1.98	302	1.007	.035	.0051
	A			.450	887.8			227	1.010	.053	.0067
	A			.300	889.8			151	1.012	.065	.0101
	A			.225	892.7			113	1.016	.083	.0135
	A			.150	903.7			75.6	1.028	.150	.0202
15.5	A	537	145.6	.600	722.7	713.5	1.94	244	1.013	.067	.0062
	A			.450	724.7			183	1.016	.082	.0082
	A			.300	728.7			122	1.021	.111	.0124
	A			.225	729.7			91.6	1.023	.119	.0165
	A			.150	742.6			61.1	1.041	.213	.0247
10.3	A	538	110.1	.600	512.0	503.0	1.86	169	1.018	.090	.0086
	A			.450	516.0			126	1.026	.130	.0115
	A			.300	520.9			84.3	1.036	.179	.0173
	A			.225	524.9			63.2	1.044	.219	.0230
	A			.150	538.8			42.1	1.071	.357	.0346
5.2	A	539	66.1	.600	290.3	276.5	1.76	90.9	1.050	.237	.0154
	A			.450	291.3			68.2	1.054	.254	.0206
	A			.300	299.2			45.5	1.082	.390	.0309
	A			.225	304.2			34.1	1.100	.476	.0412
	A			.150	321.1			22.7	1.161	.766	.0618

NACA

TABLE II.- SUMMARY OF DATA AND RESULTS FOR SUPERSONIC AIR STREAMS - Continued

Flow rate, lb/hr	Probe type	T_o, ^oR	p_2, μ Hg	d, in.	p_i, μ Hg	$p_{i(ideal)}$, μ Hg	M	Re	$\frac{p_i}{p_{i(ideal)}}$	C_{μ_2}	$1/Re_2$
Nozzle 2A											
26	B	536	189.7	0.600	1,615.4	1,623.0	2.70	683	0.995	-0.025	0.0031
	B			.450	1,613.9			513	.994	-.030	.0041
	B			.300	1,612.9			342	.994	-.034	.0062
	B			.225	1,613.9			256	.994	-.030	.0082
	B			.150	1,618.9			171	.998	-.014	.0123
	B			.100	1,629.8			114	1.004	.023	.0185
20	B	534	159.2	.600	1,287.0	1,293.0	2.62	533	.995	-.026	.0038
	B			.450	1,285.0			400	.994	-.034	.0051
	B			.300	1,285.0			267	.994	-.034	.0076
	B			.225	1,286.0			200	.995	-.030	.0102
	B			.150	1,295.0			133	1.002	.009	.0153
	B			.100	1,307.9			88.9	1.012	.063	.0230
2.3	B	534	41.8	.600	253.2	254.0	2.21	93.4	.997	-.021	.0182
	B			.450	255.7			70.0	1.007	.044	.0243
	B			.300	265.2			46.7	1.044	.295	.0364
	B			.225	273.1			35.0	1.075	.503	.0485
	B			.150	287.1			23.4	1.130	.871	.0728
	B			.100	308.0			15.6	1.213	1.420	.1092
26	C	536	191.0	.600	1,629.7	1,623.0	2.69	681	1.004	.023	.0031
	C			.450	1,632.0			511	1.006	.030	.0041
	C			.300	1,628.8			340	1.004	.020	.0062
	C			.225	1,627.5			255	1.003	.015	.0082
	C			.150	1,619.1			170	.998	-.013	.0124
	C			.100	1,608.4			114	.991	-.049	.0185
20	C	538	163.7	.600	1,293.8	1,293.0	2.57	521	1.001	.004	.0038
	C			.450	1,296.0			390	1.002	.013	.0051
	C			.300	1,293.6			260	1.000	.003	.0077
	C			.225	1,292.1			195	.999	-.004	.0102
	C			.150	1,285.5			130	.994	-.033	.0153
	C			.100	1,278.1			86.8	.988	-.065	.0230
2.3	C	539	45.8	.600	252.8	254.0	2.24	92.8	.995	-.032	.0174
	C			.450	248.3			69.6	.978	-.151	.0232
	C			.300	245.3			46.5	.966	-.230	.0347
	C			.225	243.8			34.9	.960	-.270	.0463
	C			.150	248.8			23.2	.980	-.138	.0695
	C			.100	260.7			15.5	1.026	.177	.1041
26	A	535	191.5	.600	1,618.9	1,623.0	2.68	678	.998	-.017	.0031
	A			.450	1,621.9			509	.999	-.004	.0041
	A			.300	1,619.9			339	.998	-.013	.0062
	A			.225	1,619.9			254	.998	-.013	.0082
	A			.150	1,620.9			170	.999	-.009	.0123
20	A	538	160.2	.600	1,292.5	1,923.0	2.61	527	1.000	-.003	.0038
	A			.450	1,294.5			396	1.001	.008	.0051
	A			.300	1,293.5			264	1.000	.003	.0077
	A			.225	1,295.5			198	1.002	.013	.0103
	A			.150	1,298.5			132	1.004	.029	.0154
2.3	A	538	38.8	.600	260.7	254.0	2.31	94.8	1.026	.161	.0187
	A			.450	262.7			71.1	1.034	.209	.0250
	A			.300	270.6			47.4	1.065	.399	.0374
	A			.225	276.6			35.6	1.089	.543	.0499
	A			.150	290.5			23.7	1.144	.877	.0749

NACA

TABLE II.- SUMMARY OF DATA AND RESULTS FOR SUPERSONIC AIR STREAMS - Concluded

Flow rate, lb/hr	Probe type	T_o, °R	p_2, μ Hg	d, in.	p_i, μ Hg	$p_{i(ideal)}$, μ Hg	M	Re	$\frac{p_i}{p_{i(ideal)}}$	C_{μ_2}	$1/Re_2$
Nozzle 3											
16.8	A	537	111.4	0.600	1,376.1	1,376	3.35	728	1.000	0.001	0.0039
	A			.450	1,378.1			546	1.002	.012	.0052
	A			.300	1,374.1			364	.999	-.011	.0078
	A			.225	1,376.1			273	1.000	.001	.0104
	A			.150	1,378.1			182	1.002	.012	.0156
10.3	A	539	88.1	.600	1,029.8	1,034	3.25	526	.996	-.032	.0052
	A			.450	1,033.8			394	1.000	-.002	.0069
	A			.300	1,033.8			263	1.000	-.002	.0104
	A			.225	1,034.8			197	1.001	.006	.0138
	A			.150	1,042.8			131	1.008	.066	.0207
4.1	A	533	53.7	.600	527.4	527	2.93	243	1.001	.006	.0097
	A			.450	531.3			182	1.008	.059	.0129
	A			.300	535.3			121	1.016	.114	.0194
	A			.225	540.3			91.1	1.025	.183	.0258
	A			.150	556.2			60.7	1.055	.403	.0387
16.8	B	541	118.9	.600	1,374.6	1,376	3.23	688	.999	-.008	.0039
	B			.450	1,371.6			516	.997	-.025	.0052
	B			.300	1,368.1			344	.994	-.044	.0078
	B			.225	1,366.6			258	.993	-.053	.0104
	B			.150	1,377.6			172	1.001	.002	.0156
	B			.100	1,391.5			115	1.011	.087	.0234
10.3	B	538	90.2	.600	1,029.8	1,034	3.21	519	.996	-.031	.0051
	B			.450	1,028.8			390	.995	-.039	.0068
	B			.300	1,029.8			260	.996	-.031	.0103
	B			.225	1,031.3			195	.997	-.020	.0137
	B			.150	1,044.8			130	1.010	.081	.0205
	B			.100	1,060.7			86.6	1.026	.199	.0308
4.1	B	536	51.7	.600	521.9	527	3.00	246	.990	-.071	.0098
	B			.450	522.4			185	.991	-.064	.0131
	B			.300	528.8			123	1.003	.025	.0196
	B			.225	536.8			92.3	1.019	.137	.0262
	B			.150	554.2			61.5	1.052	.381	.0393
	B			.100	576.1			41.0	1.093	.688	.0589
16.8	C	535	111.1	.600	1,369.2	1,376	3.36	737	.995	-.039	.0039
	C			.450	1,372.0			553	.997	-.023	.0052
	C			.300	1,372.9			368	.998	-.018	.0078
	C			.225	1,371.6			276	.997	-.025	.0104
	C			.150	1,367.3			184	.994	-.050	.0156
	C			.100	1,360.5			123	.989	-.089	.0233
10.3	C	535	92.2	.600	1,041.6	1,034	3.17	517	1.007	.056	.0051
	C			.450	1,039.0			388	1.005	.037	.0068
	C			.300	1,036.9			259	1.003	.021	.0102
	C			.225	1,032.9			194	.999	-.008	.0135
	C			.150	1,026.8			129	.993	-.053	.0203
	C			.100	1,022.9			86.2	.989	-.082	.0305
4.1	C	536	56.4	.600	528.5	527	2.84	232	1.003	.020	.0097
	C			.450	525.4			174	.997	-.022	.0129
	C			.300	520.9			116	.988	-.082	.0193
	C			.225	518.9			86.9	.985	-.109	.0258
	C			.150	516.4			58.0	.980	-.143	.0386
	C			.100	521.9			38.6	.990	-.069	.0580

NACA

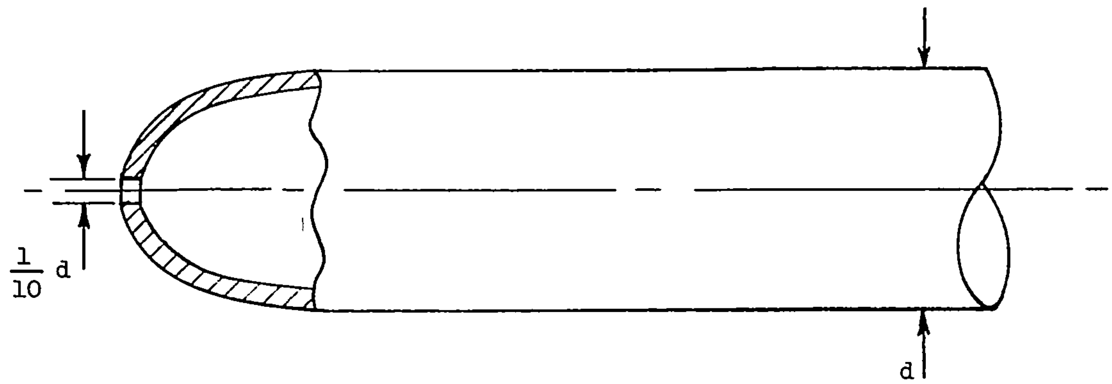

(a) Type A. Ten-to-one source-shaped tube.

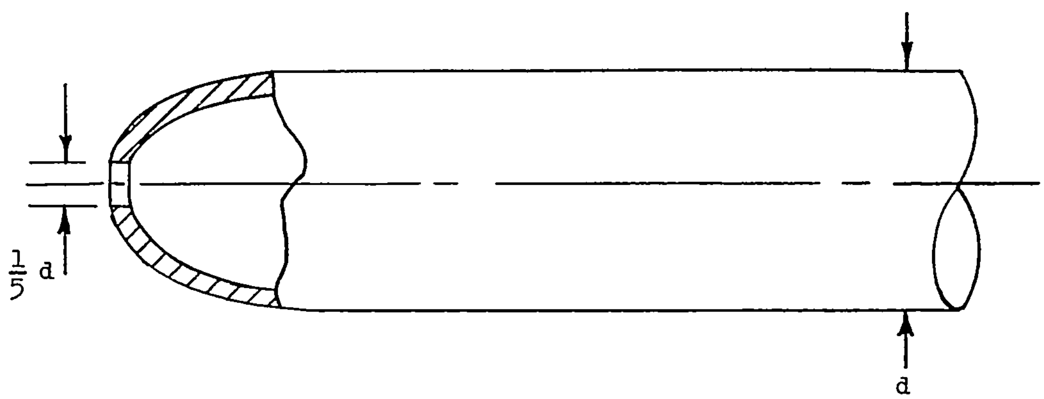

(b) Type B. Five-to-one source-shaped tube.

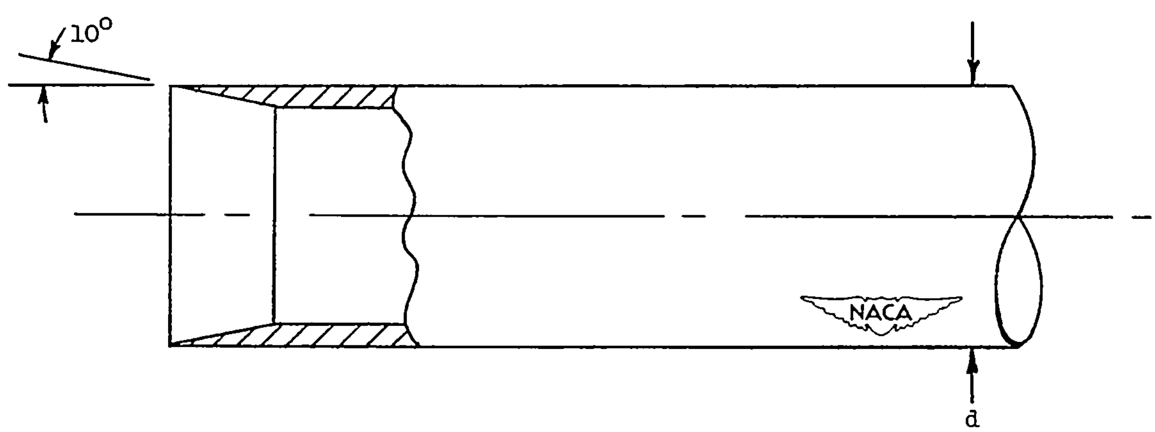

(c) Type C. Open-ended tube.

Figure 1.- Impact-probe geometry.

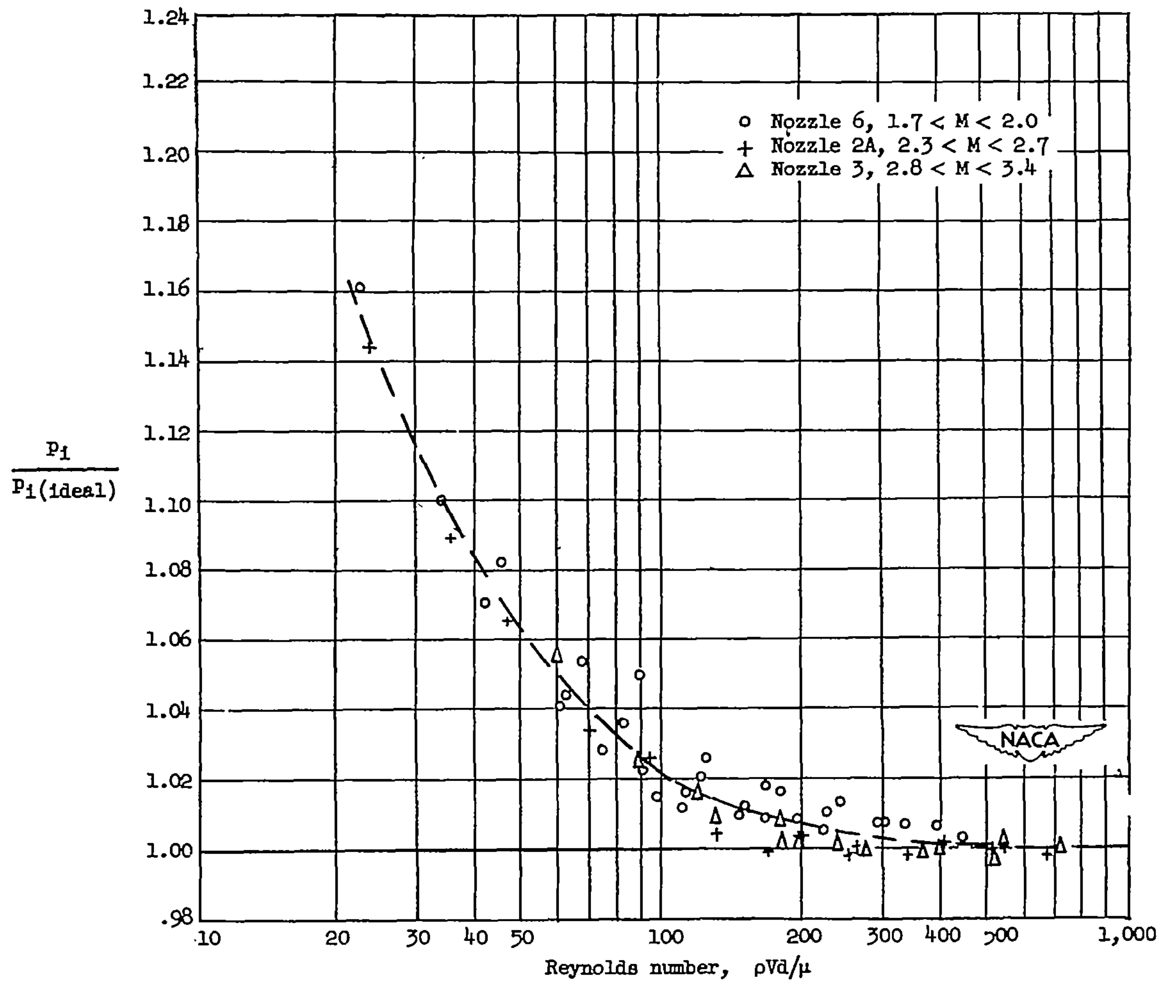

(a) Type A probes.

Figure 2.- Correction factors for impact-pressure measurements. Supersonic air stream.

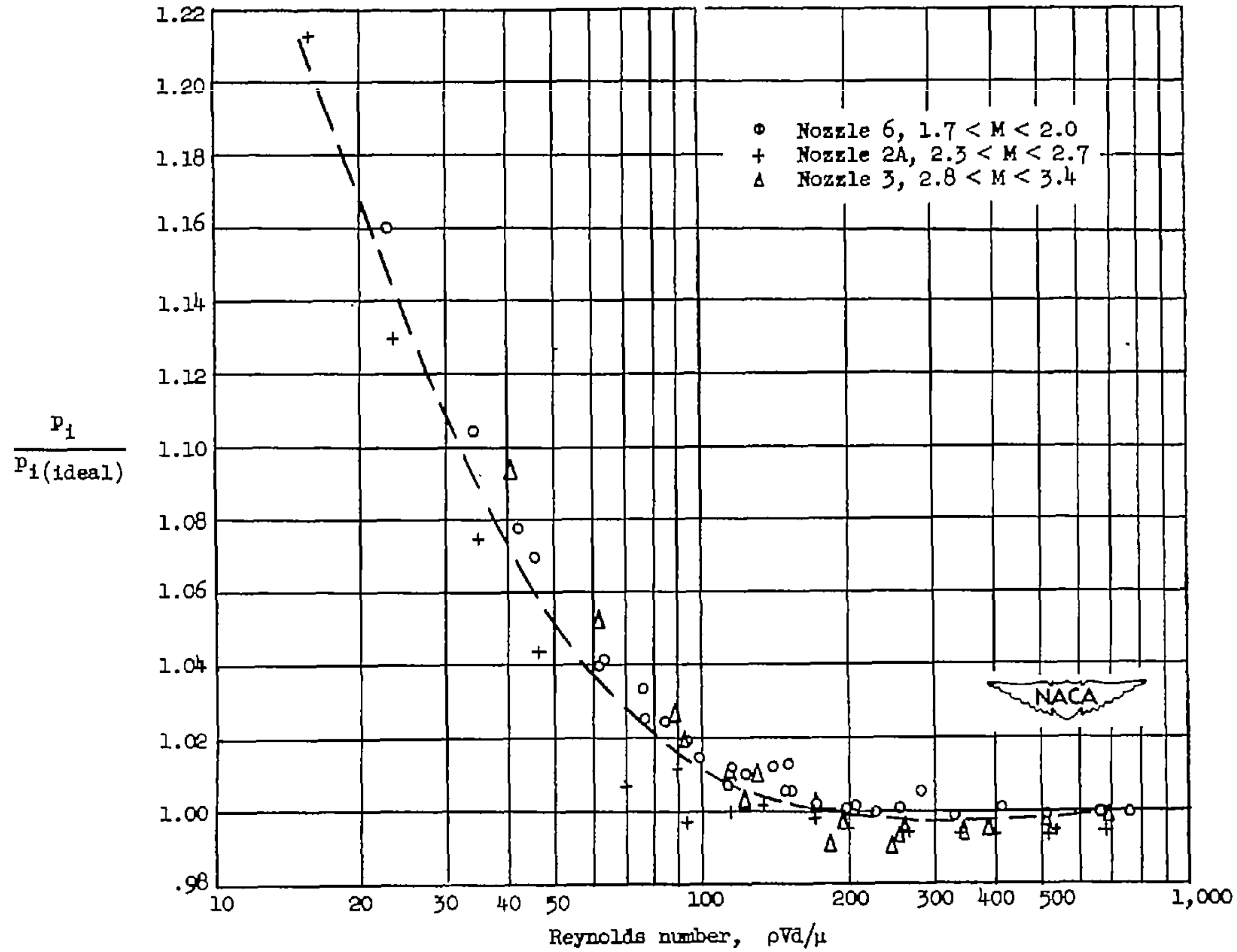

(b) Type B probes.

Figure 2.- Continued.

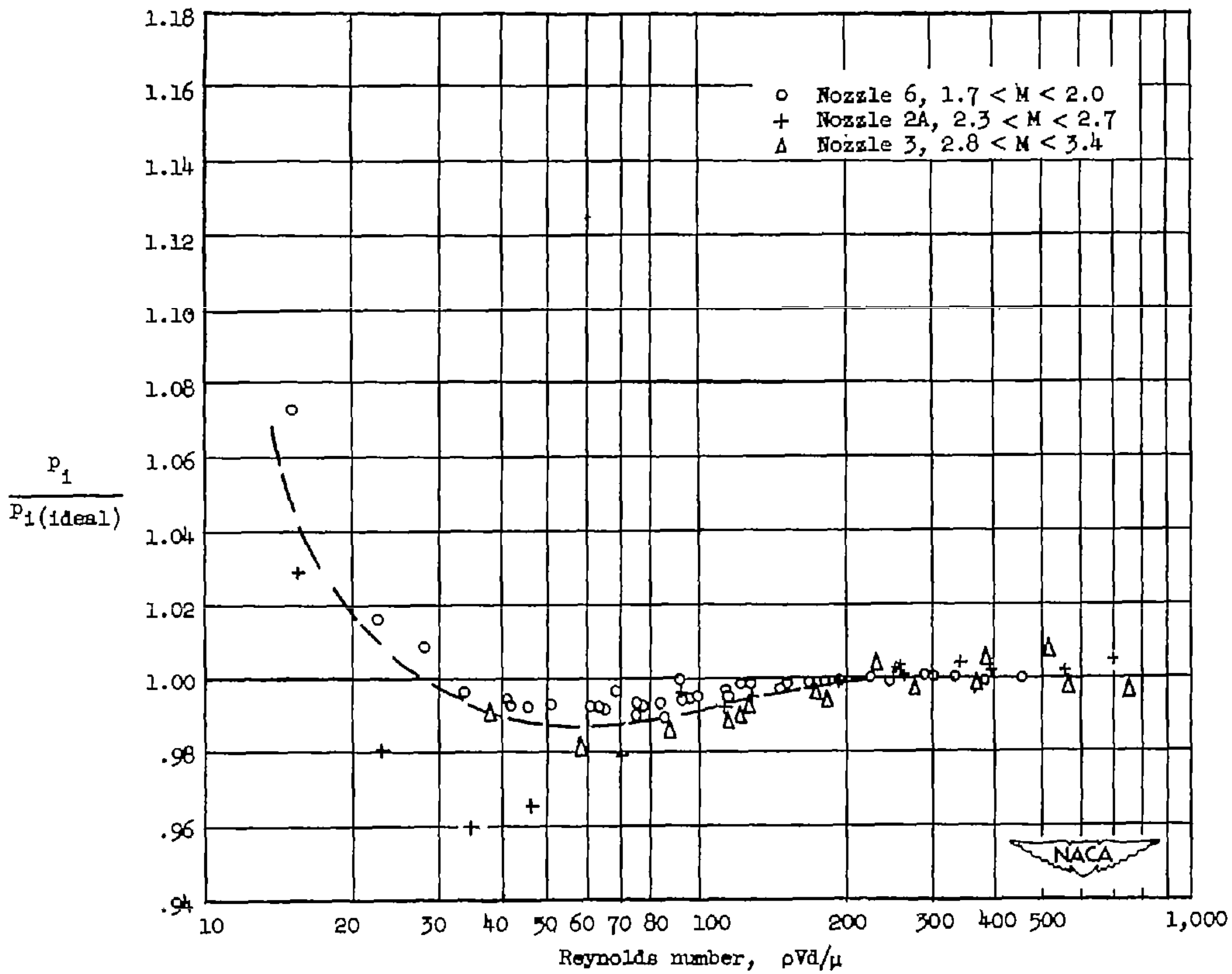

(c) Type C probes.

Figure 2.- Concluded.

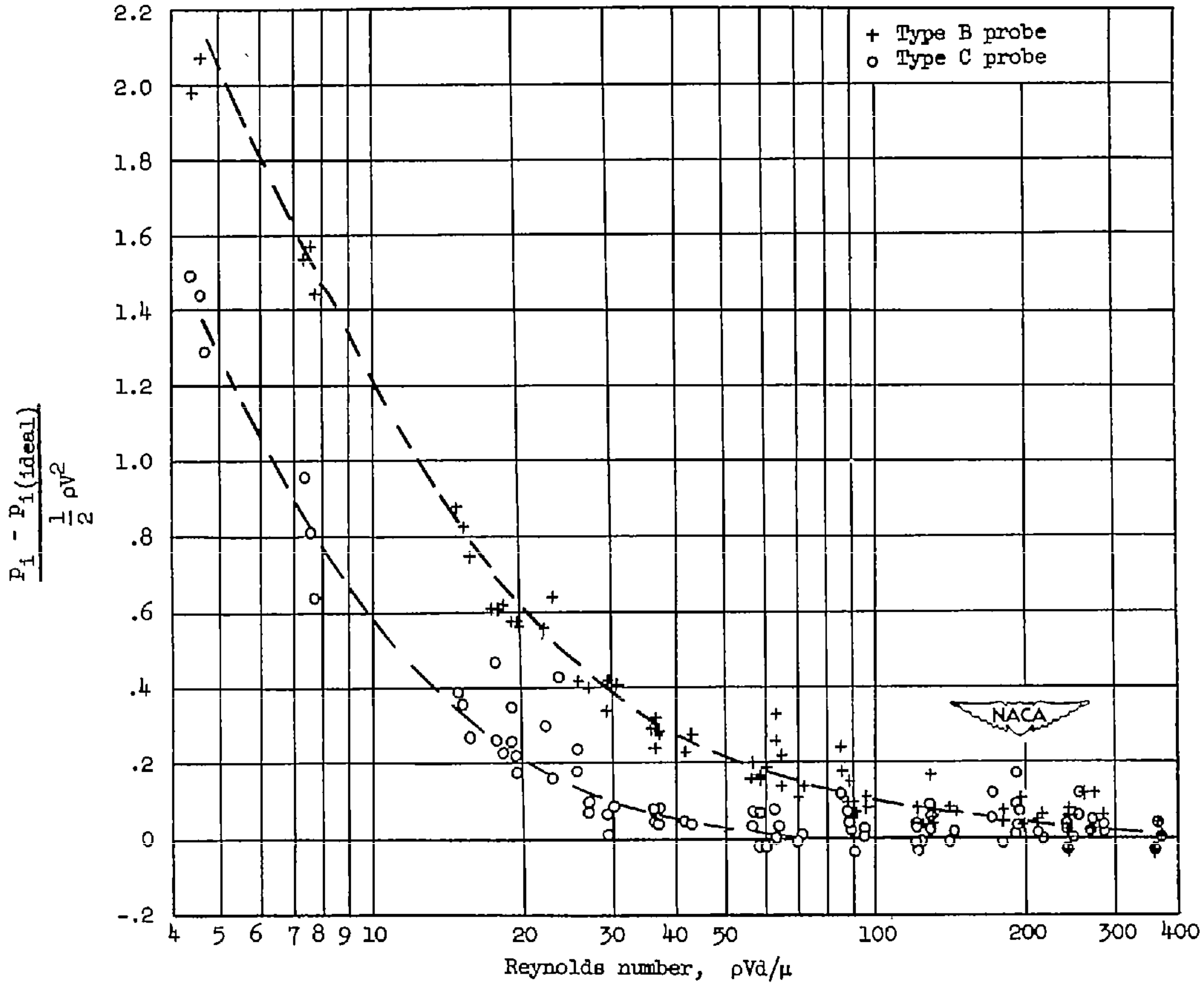

Figure 3.- Pressure coefficient of viscosity effect. Type B and C impact probes. Subsonic air stream $(0.10 < M < 0.67)$.

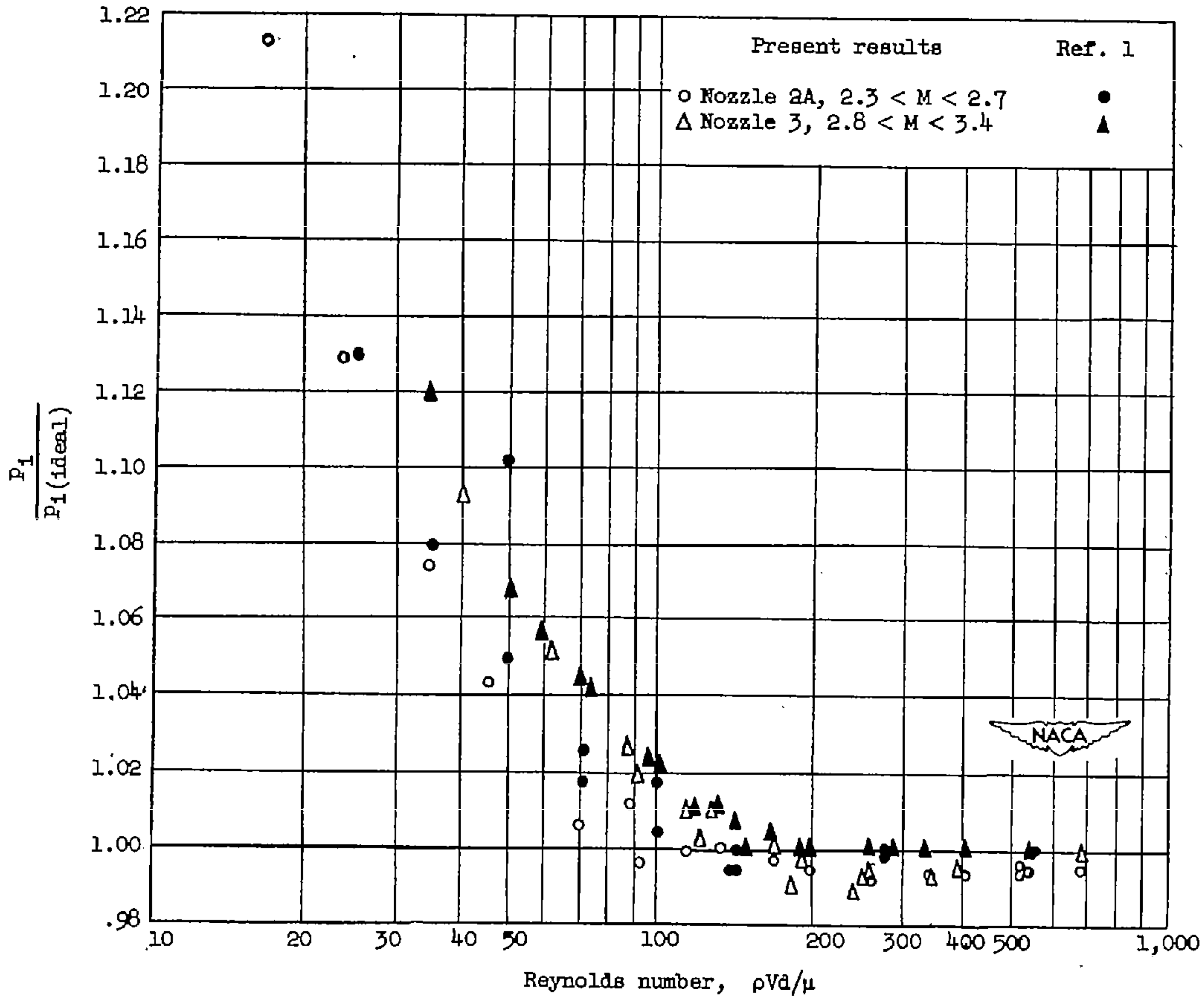

Figure 4.- Comparison of present results with those of reference 1. Type B probes.

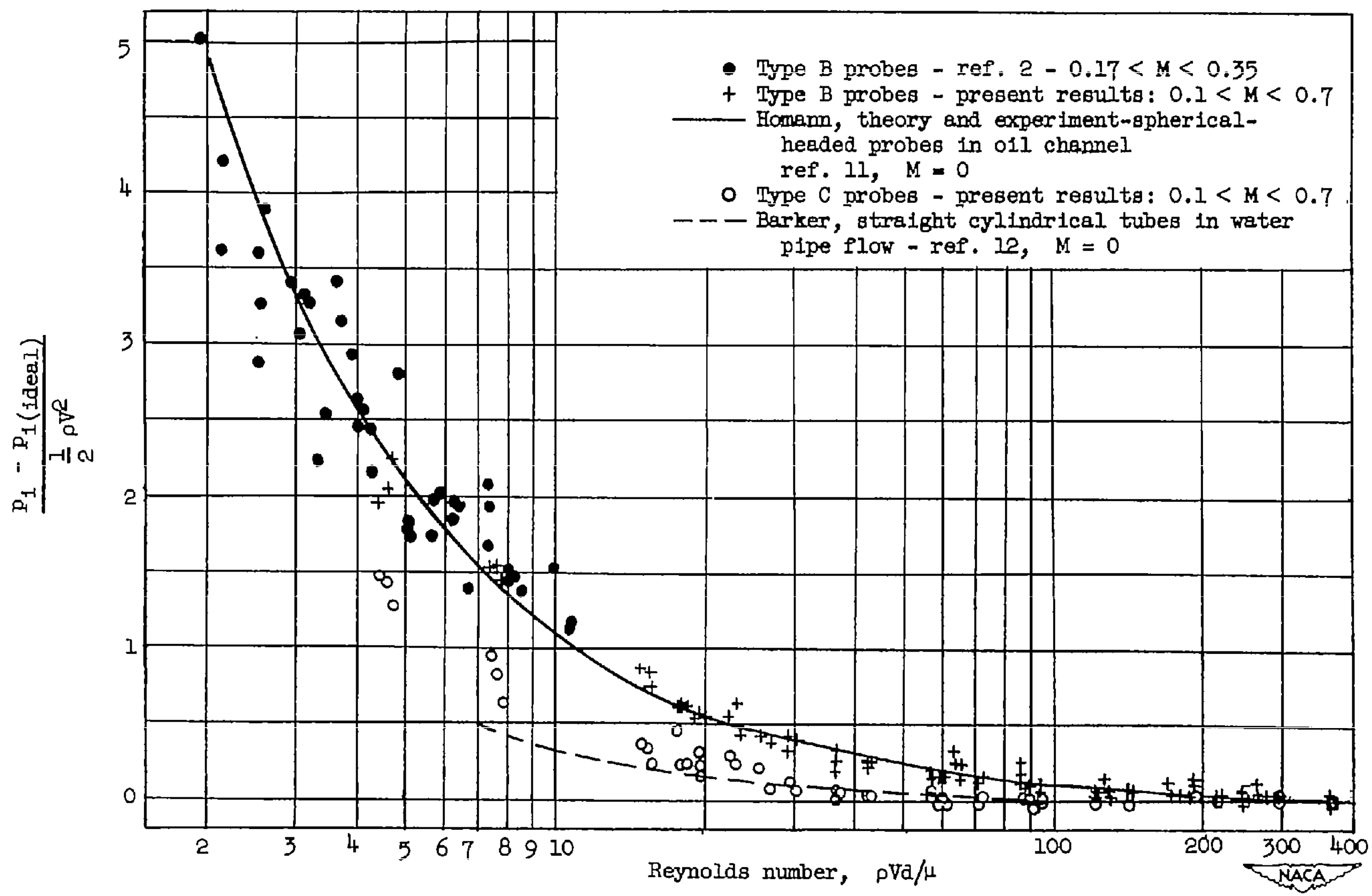

Figure 5.- Comparison of present and past results for subsonic flows.

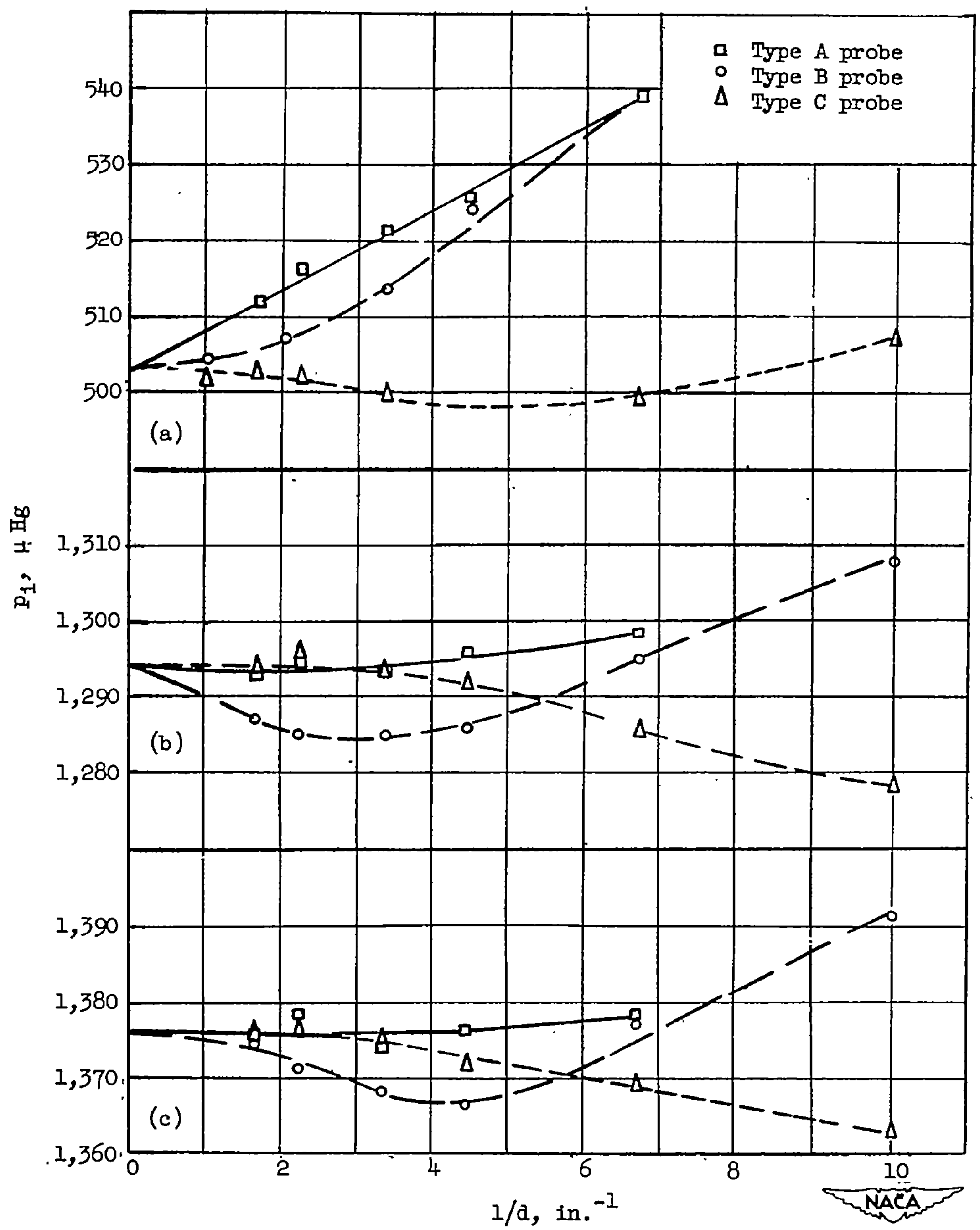

(a) Nozzle 6. 10.3 pounds per hour; M = 1.86; Re = 288 per inch.

(b) Nozzle 2A. 20 pounds per hour; M = 2.62; Re = 890 per inch.

(c) Nozzle 3. 16.8 pounds per hour; M = 3.35; Re = 1,230 per inch.

Figure 6.- Sample plots of p_i against 1/d. Supersonic air stream.

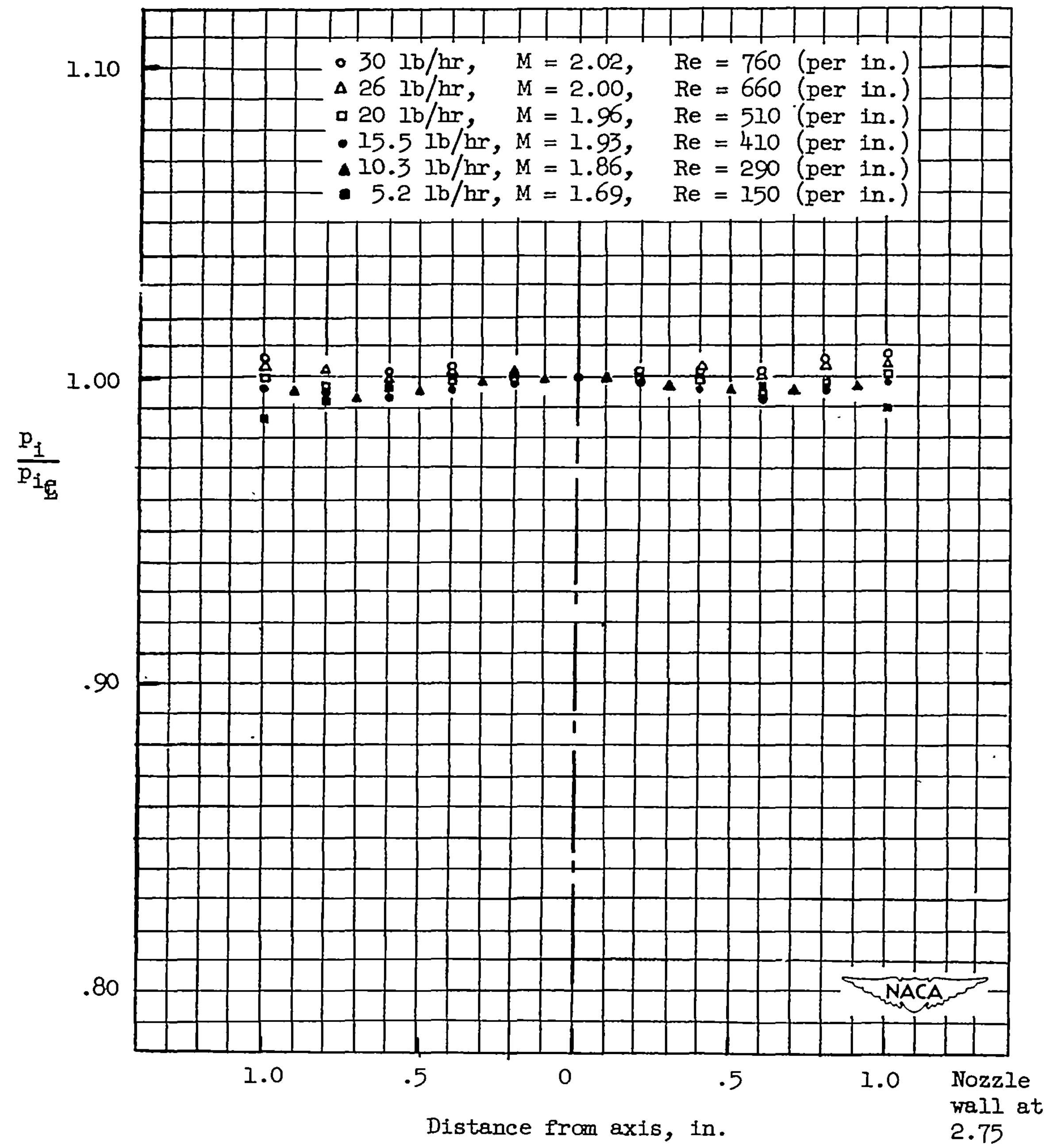

(a) Nozzle 6.

Figure 7.- Radial distribution of impact pressures. No. 3 wind tunnel.

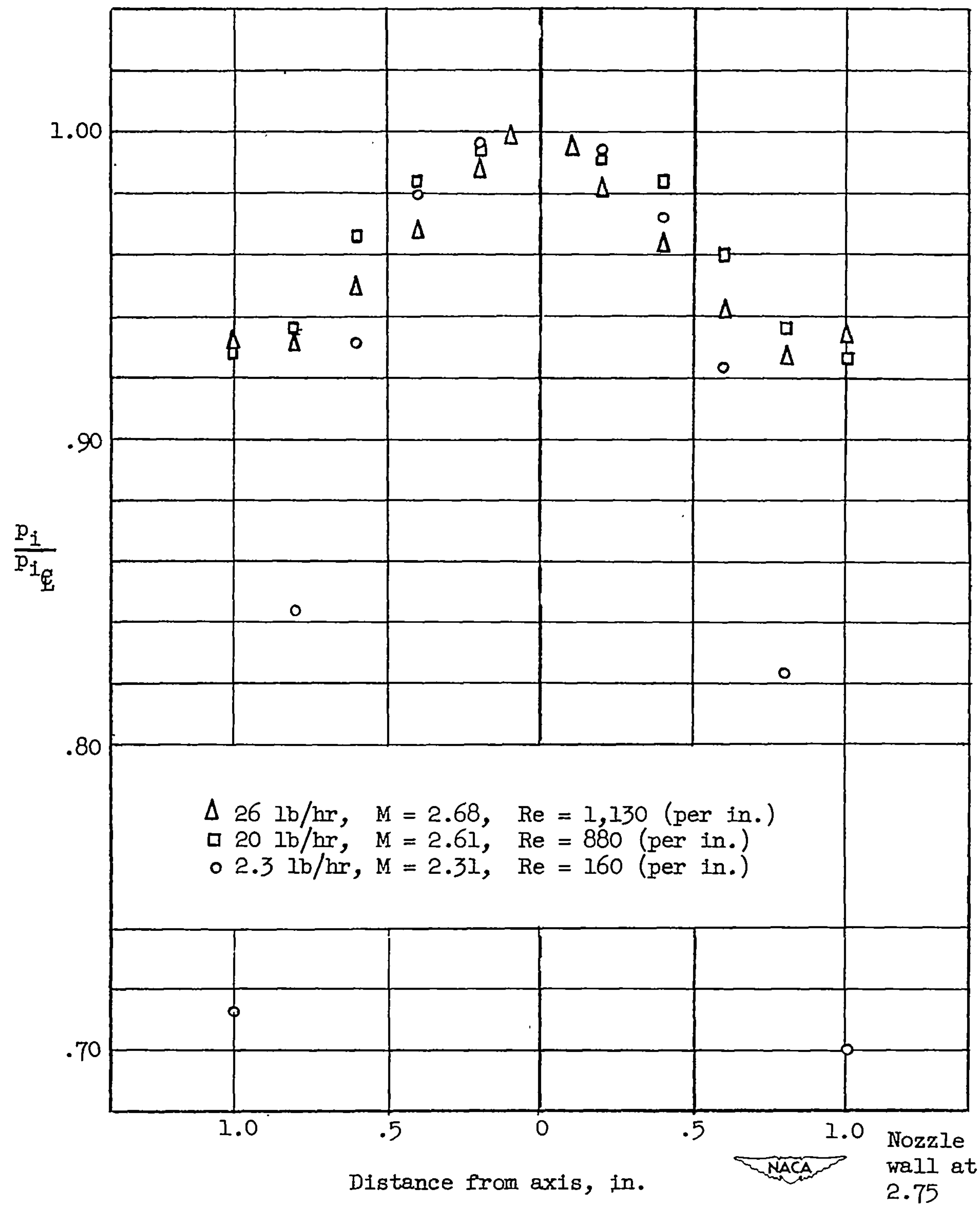

(b) Nozzle 2A.

Figure 7.- Continued.

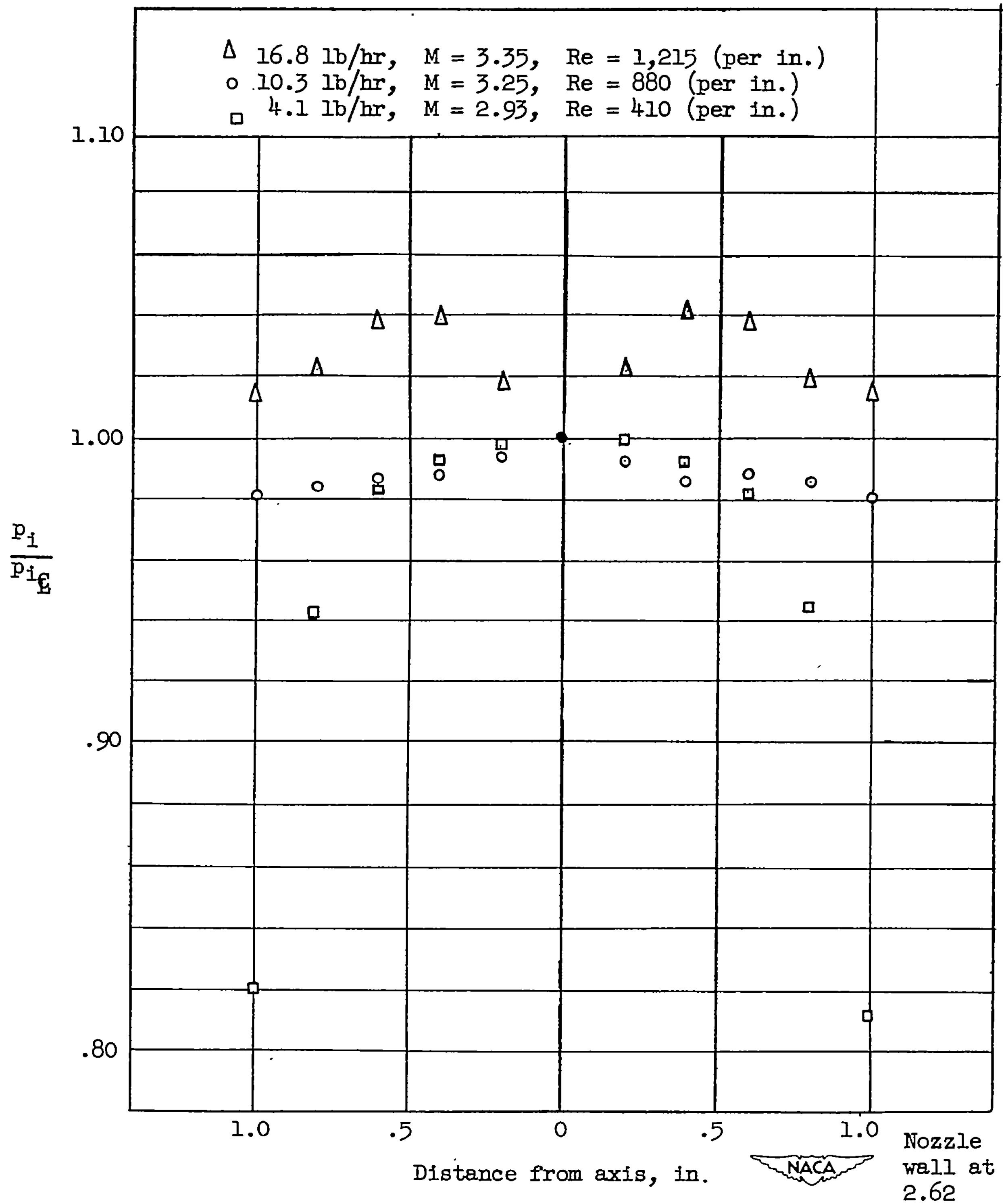

(c) Nozzle 3.

Figure 7.- Concluded.

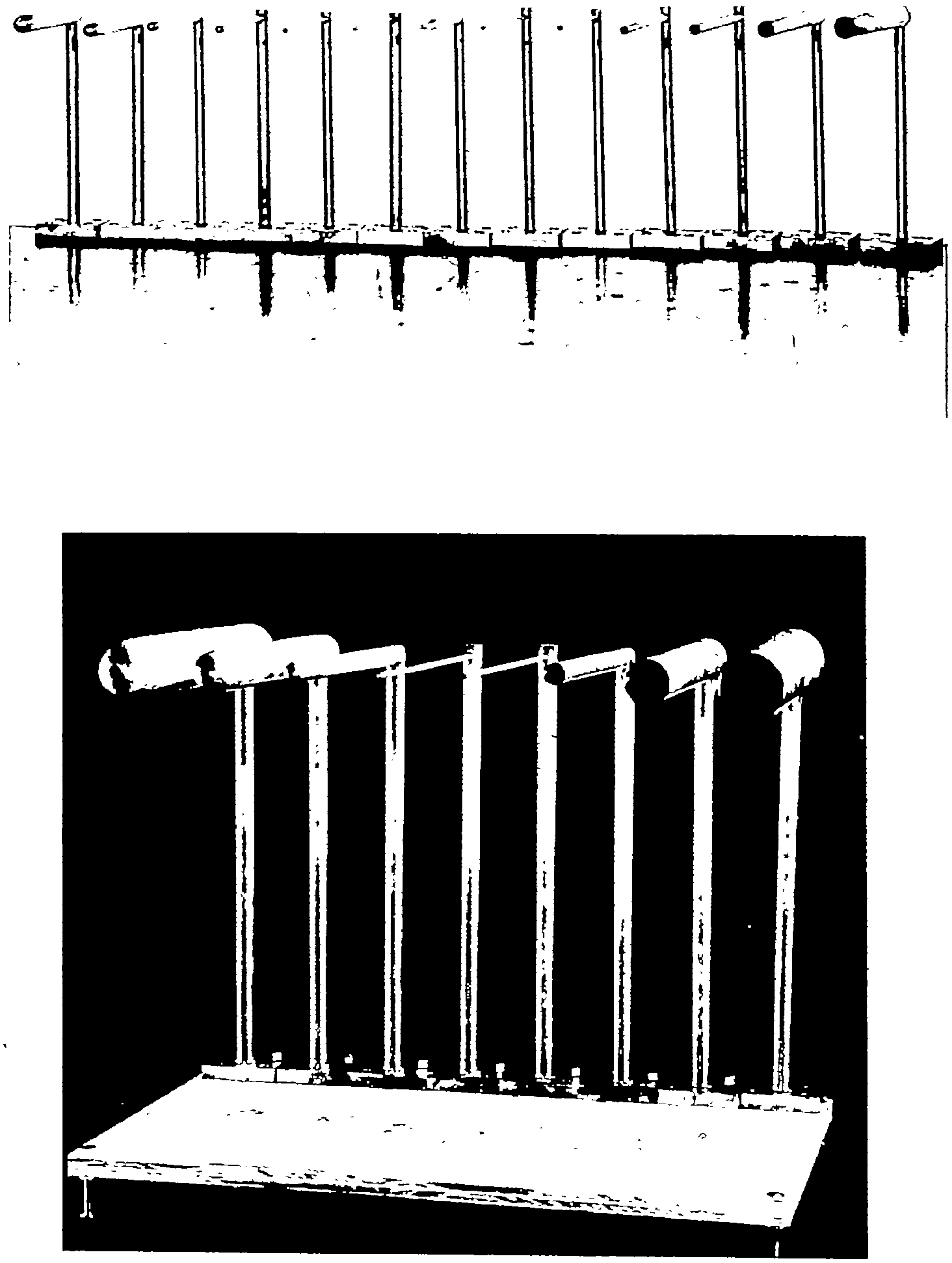

L-80233

Figure 8.- Representative groups of impact probes used in supersonic and subsonic air streams.

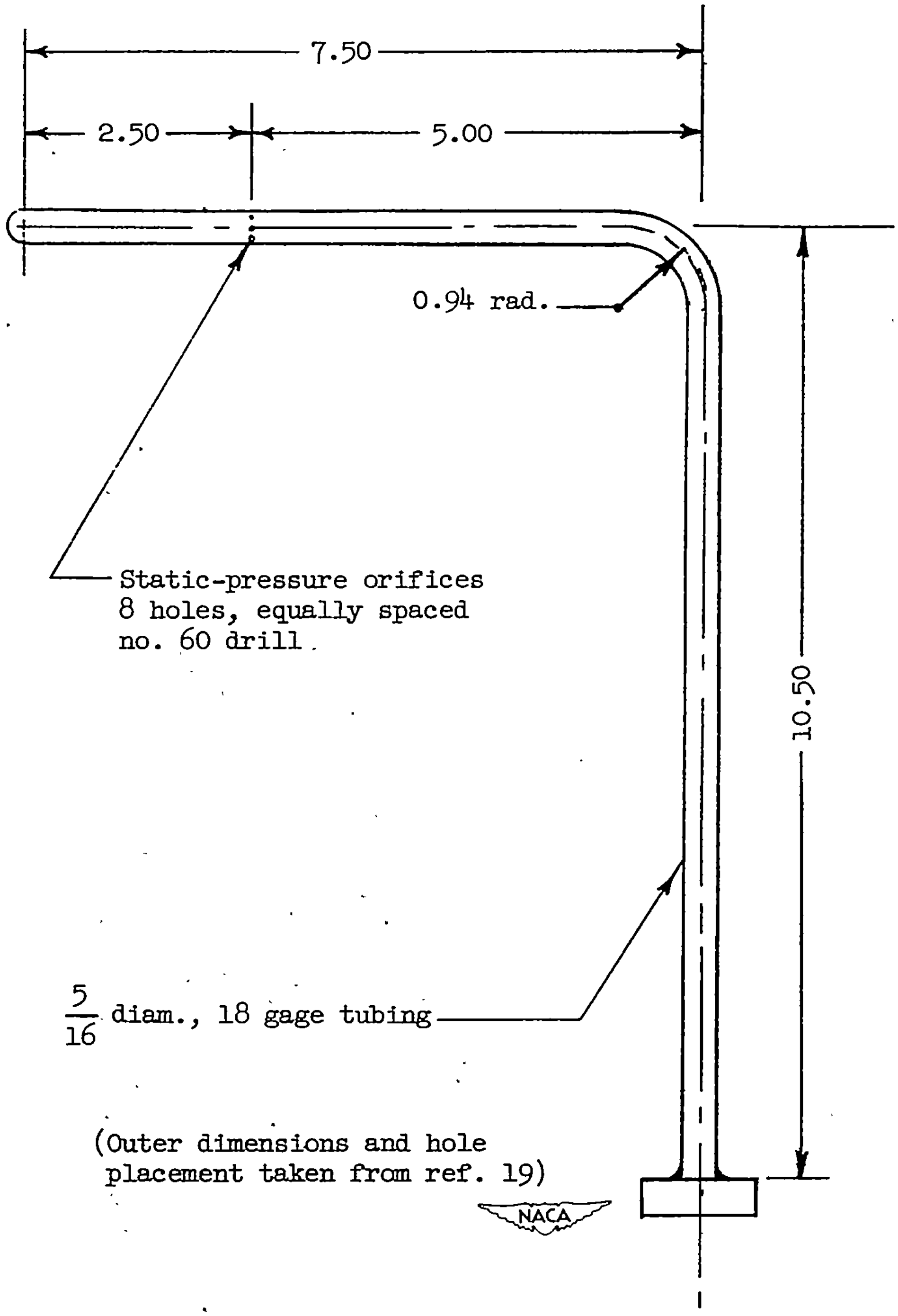

Figure 9.- Subsonic static probe. All dimensions are in inches.

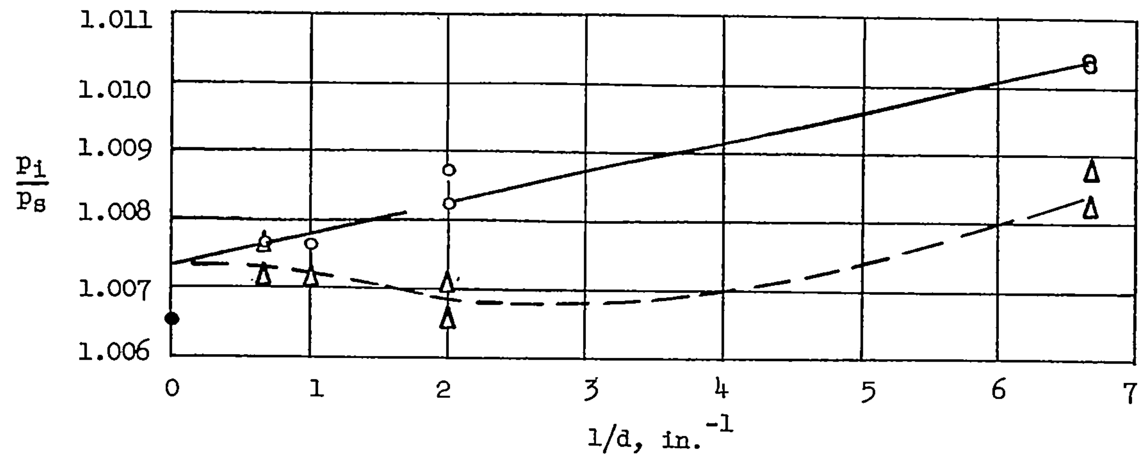

(a) Point 3. M = 0.097; Re = 128 (per inch).

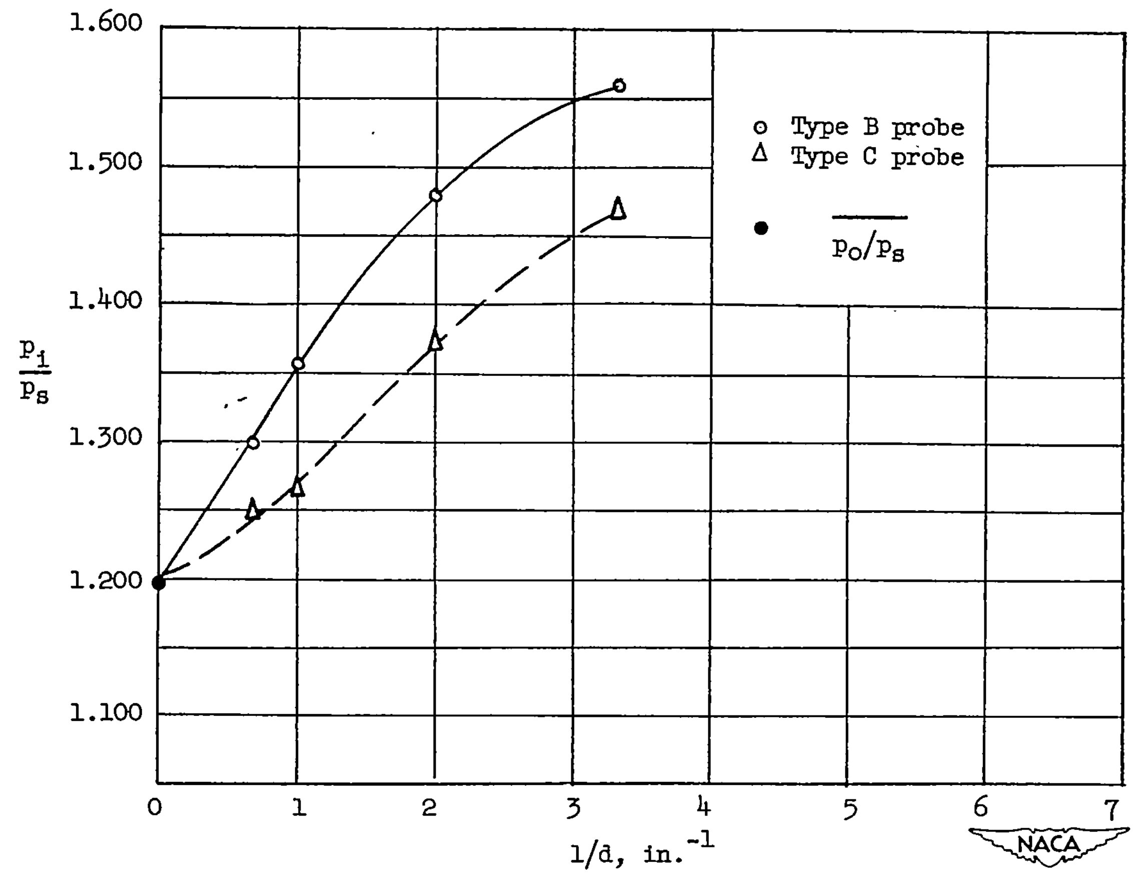

(b) Point 24. M = 0.512; Re = 14.8 (per inch).

Figure 10.- Sample plots of p_i/p_s against $1/d$. Subsonic air stream.

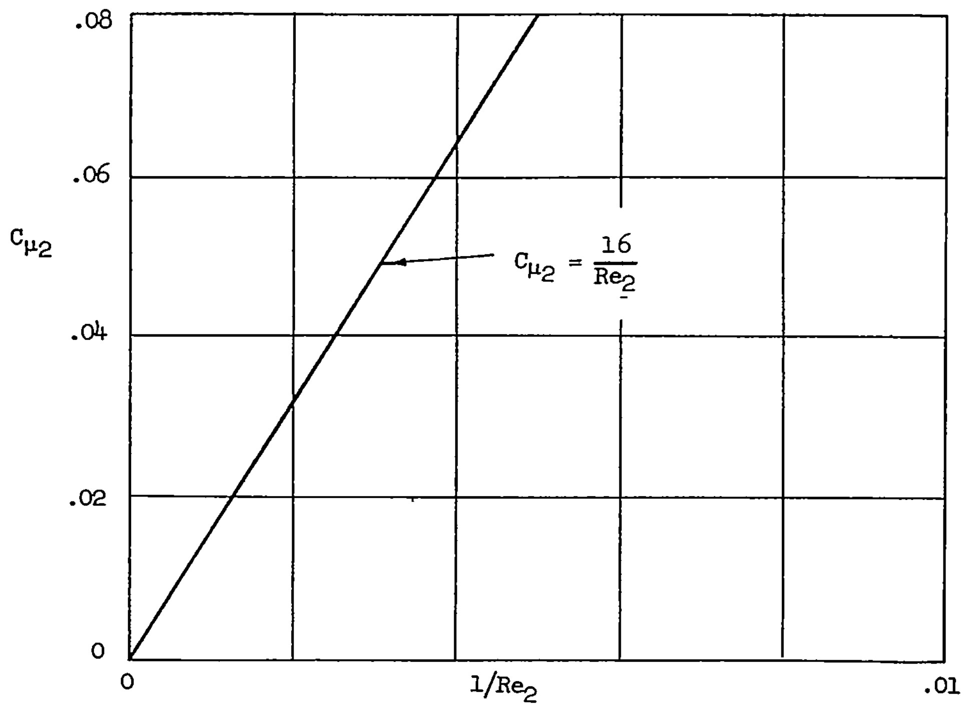

(a) C_{μ_2} against $1/Re_2$.

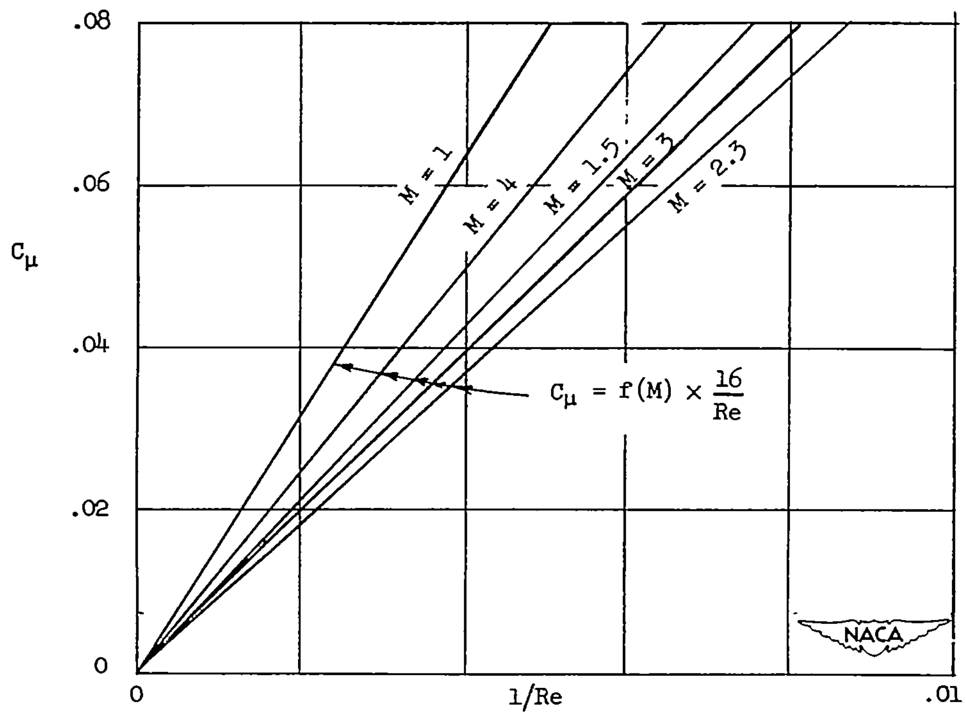

(b) C_μ against $1/Re$.

Figure 11.- Various presentations of incompressible-fluid theory for a source-shaped tube.

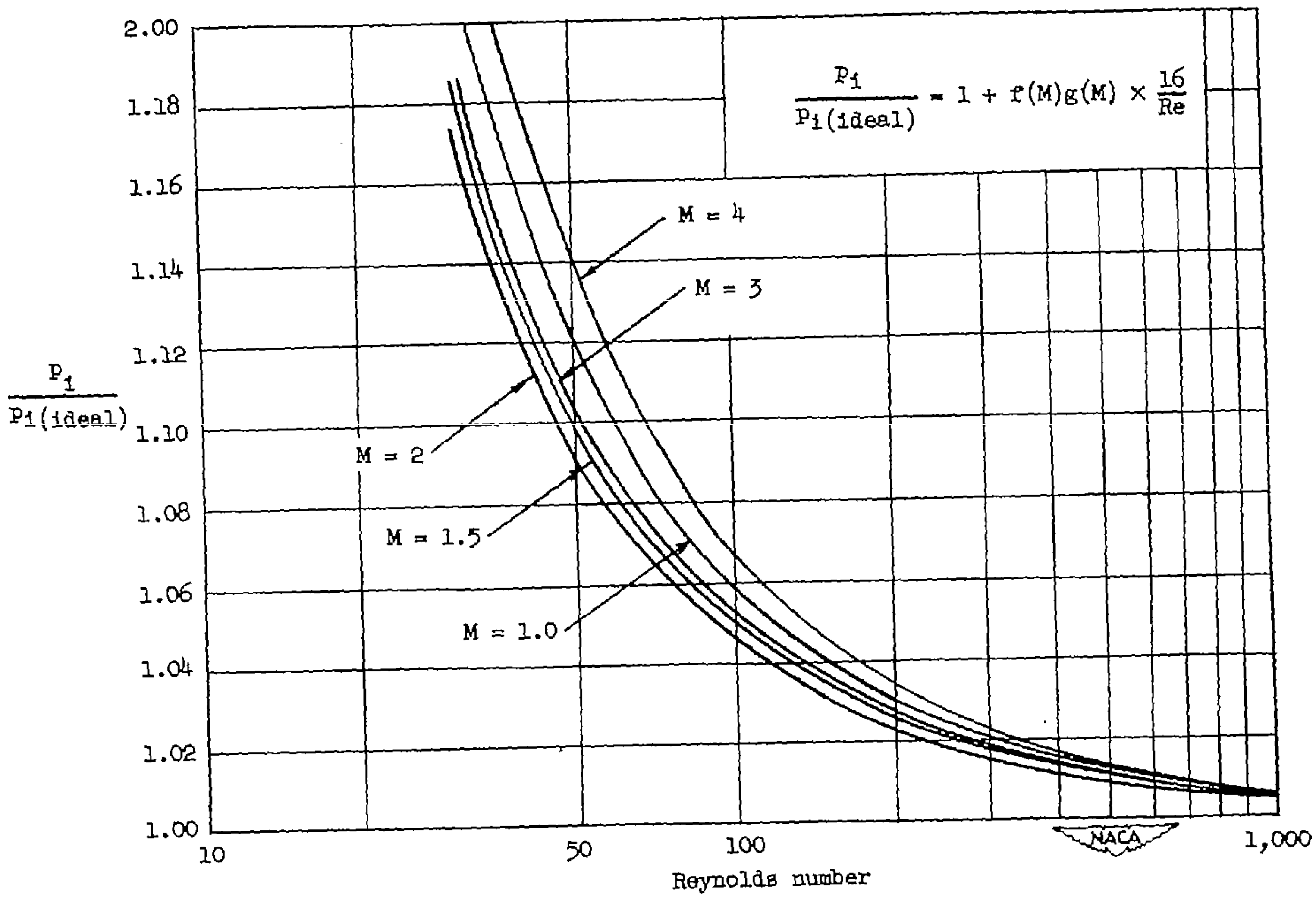

(c) $p_i/p_{i(ideal)}$ against Re.

Figure 11.- Concluded.

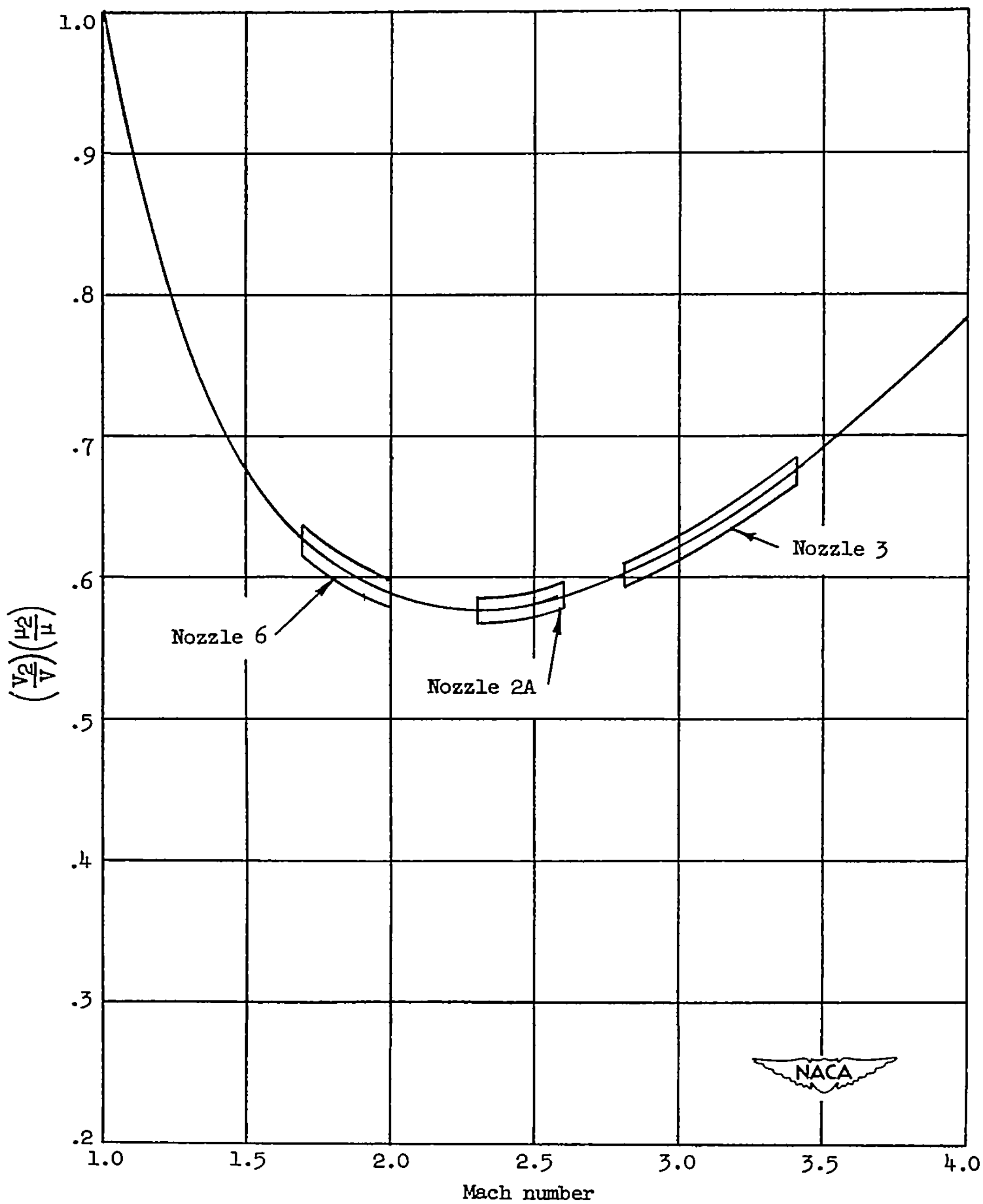

Figure 12.- Function of a normal shock wave. Assumed upstream reservoir temperature T_0, 70° F. $f(M) = \left(\frac{V_2}{V}\right)\left(\frac{\mu_2}{\mu}\right)$

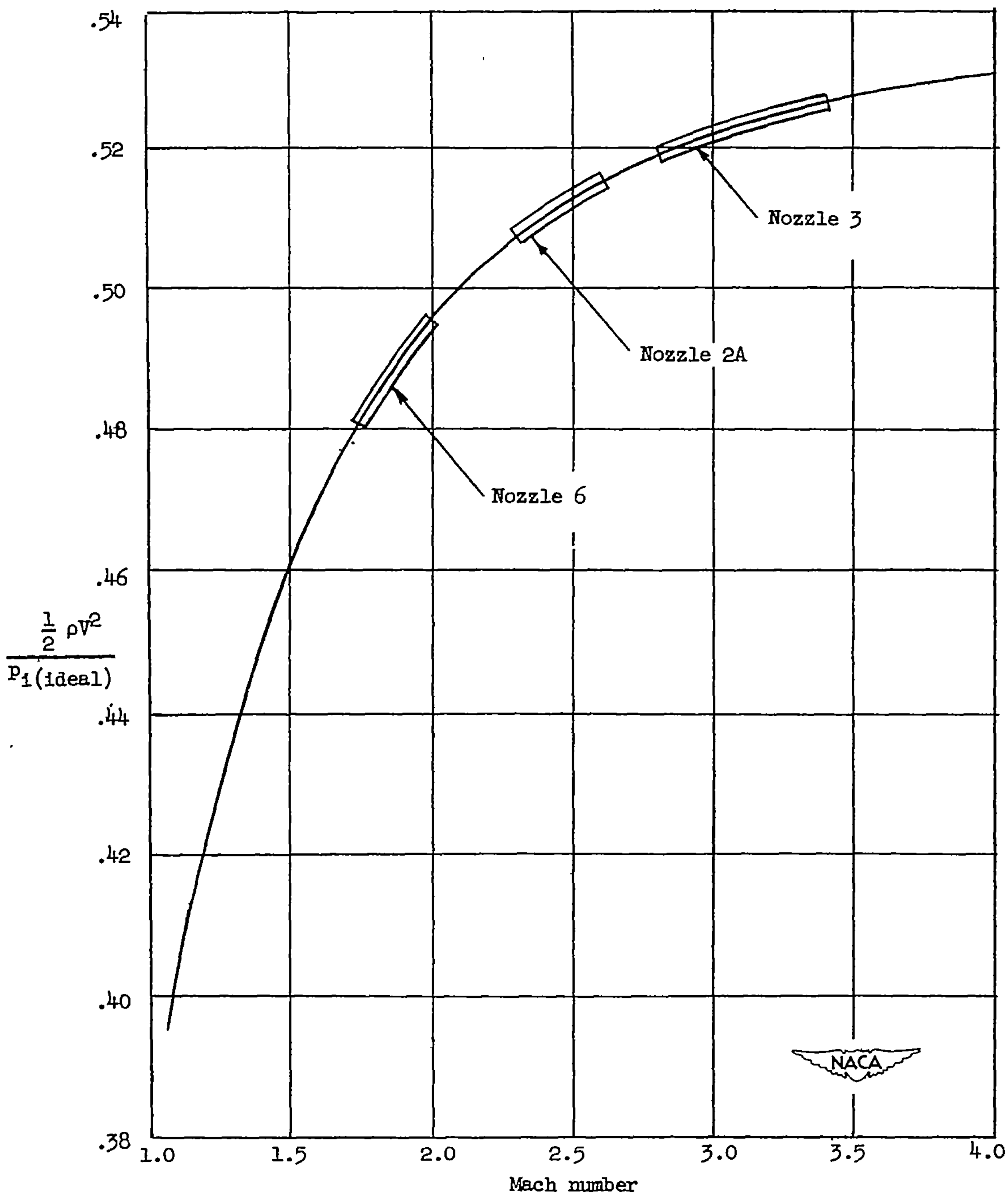

Figure 13.- Ratio of dynamic pressure to ideal impact pressure. Supersonic air streams. $g(M) = \dfrac{\frac{1}{2}\rho V^2}{p_{i(ideal)}}$.

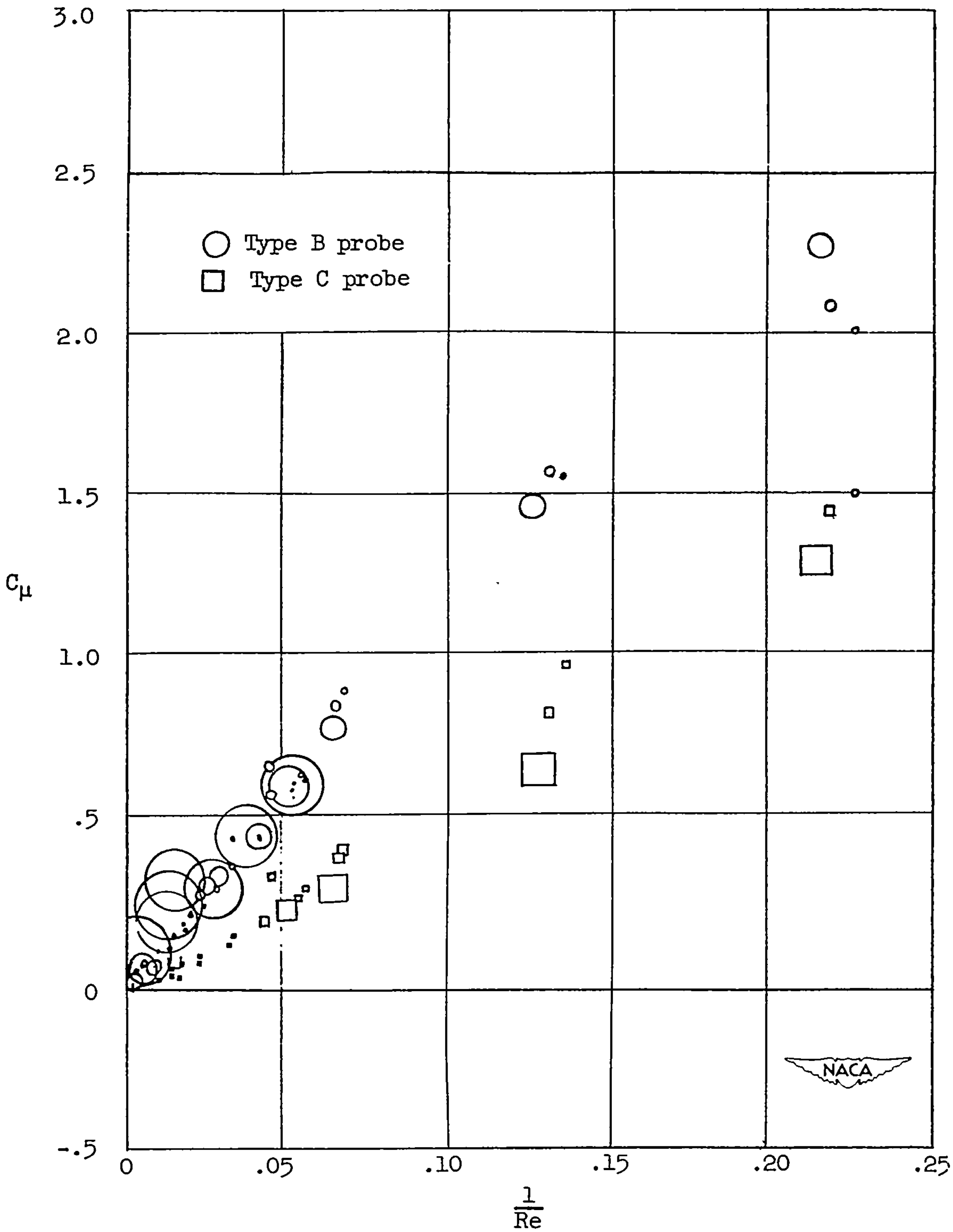

Figure 14.- Viscous effect on subsonic impact pressures showing probable error of measurements.

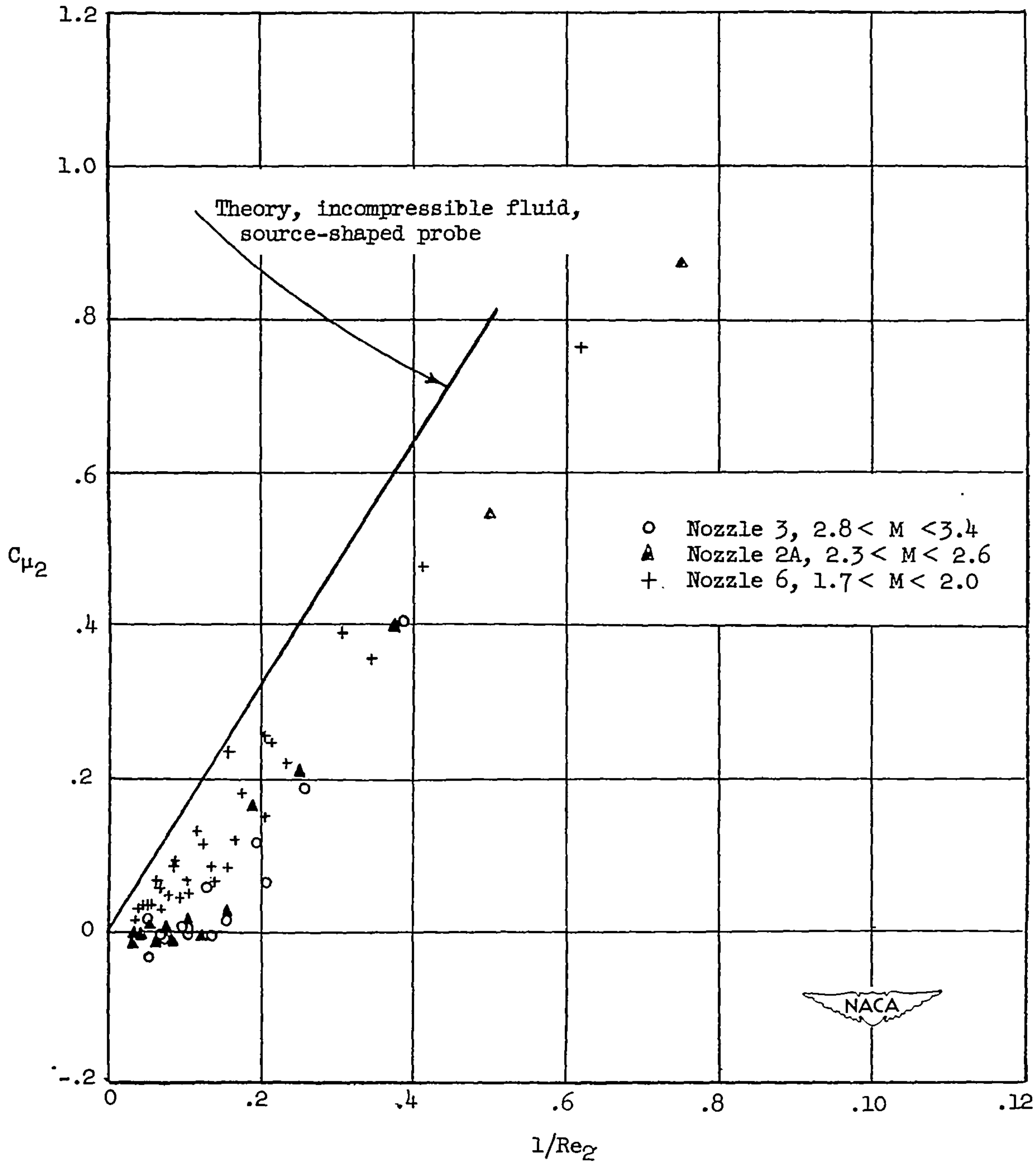

(a) Type A probes. (This probe type was not tested in subsonic air streams.)

Figure 15.- Graphs of C_{μ_2} against $1/Re_2$.

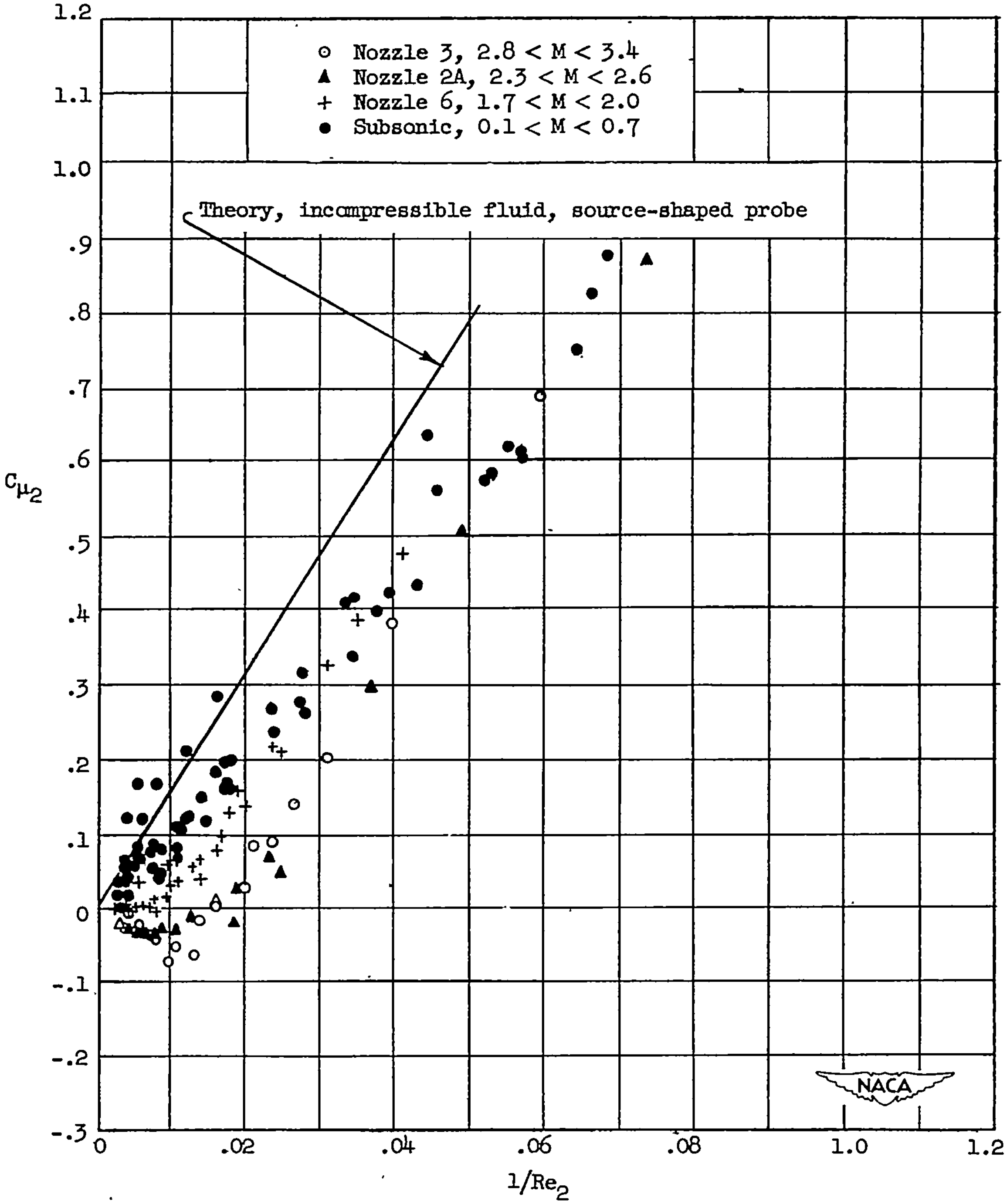

(b) Type B probes.

Figure 15.- Continued.

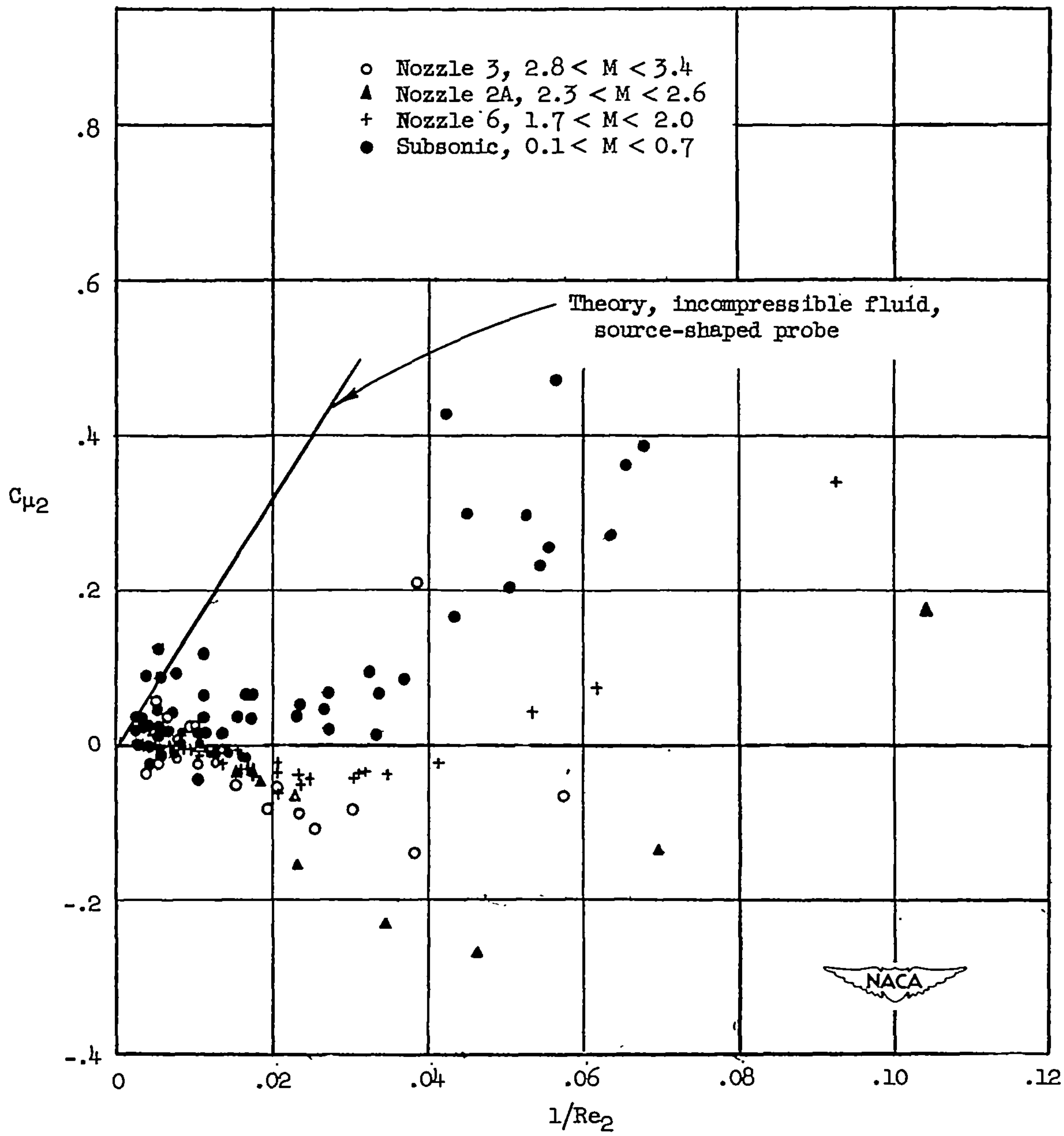

(c) Type C probes.

Figure 15.- Concluded.

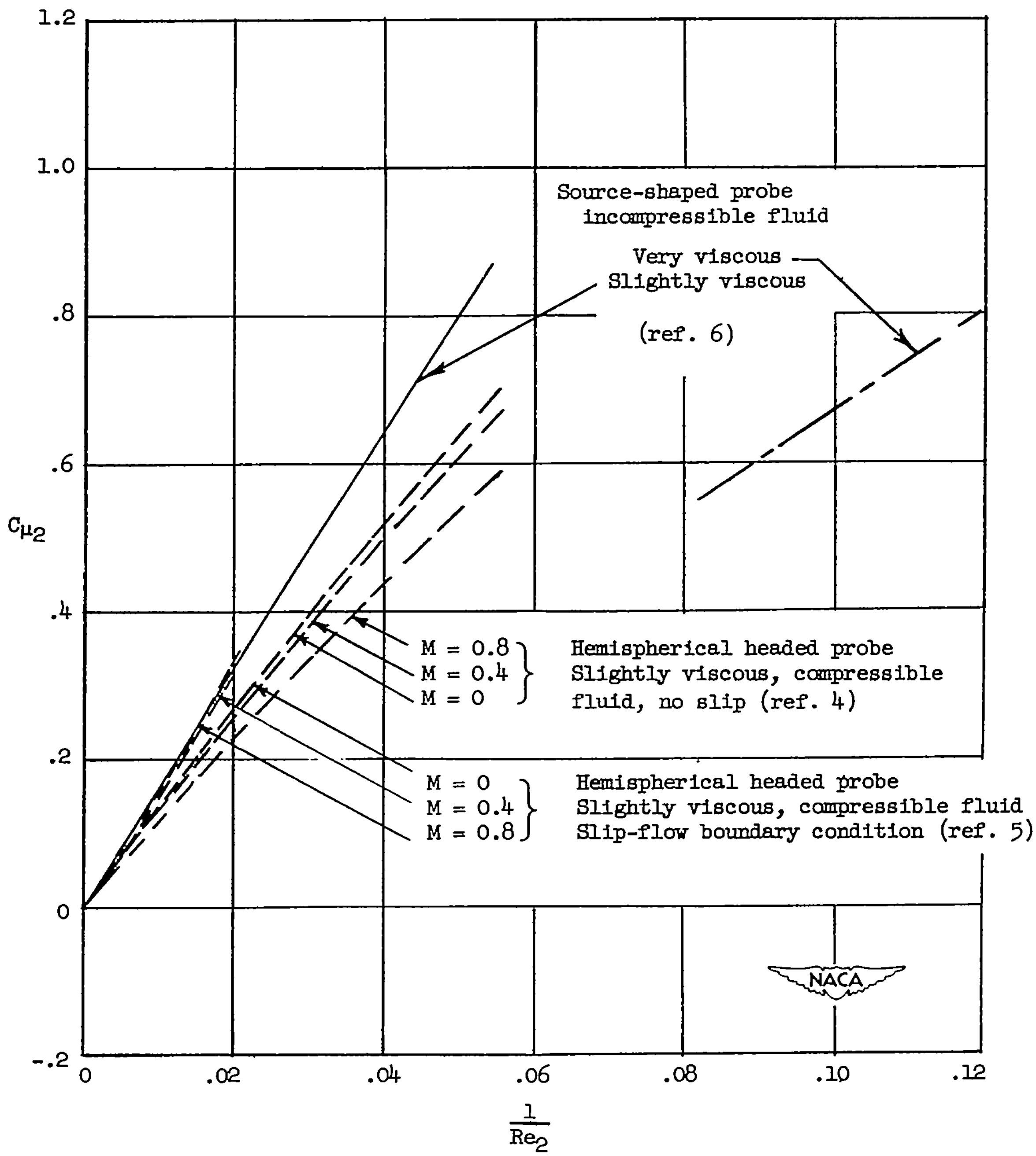

Figure 16.- Comparison of various theories.

L-80234

Figure 17.- General appearance of special McLeod gage.

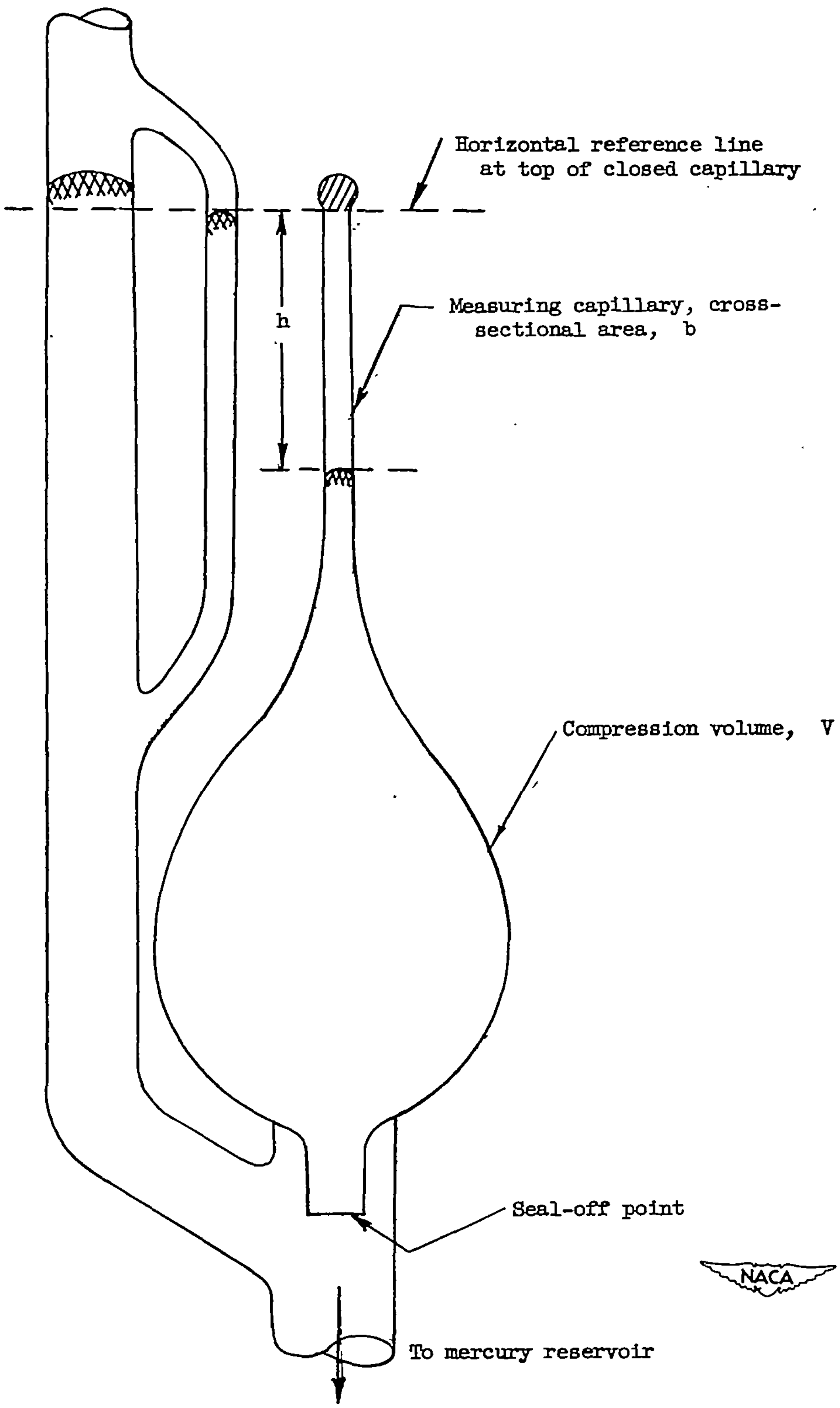

Figure 18.- Schematic diagram of McLeod gage.

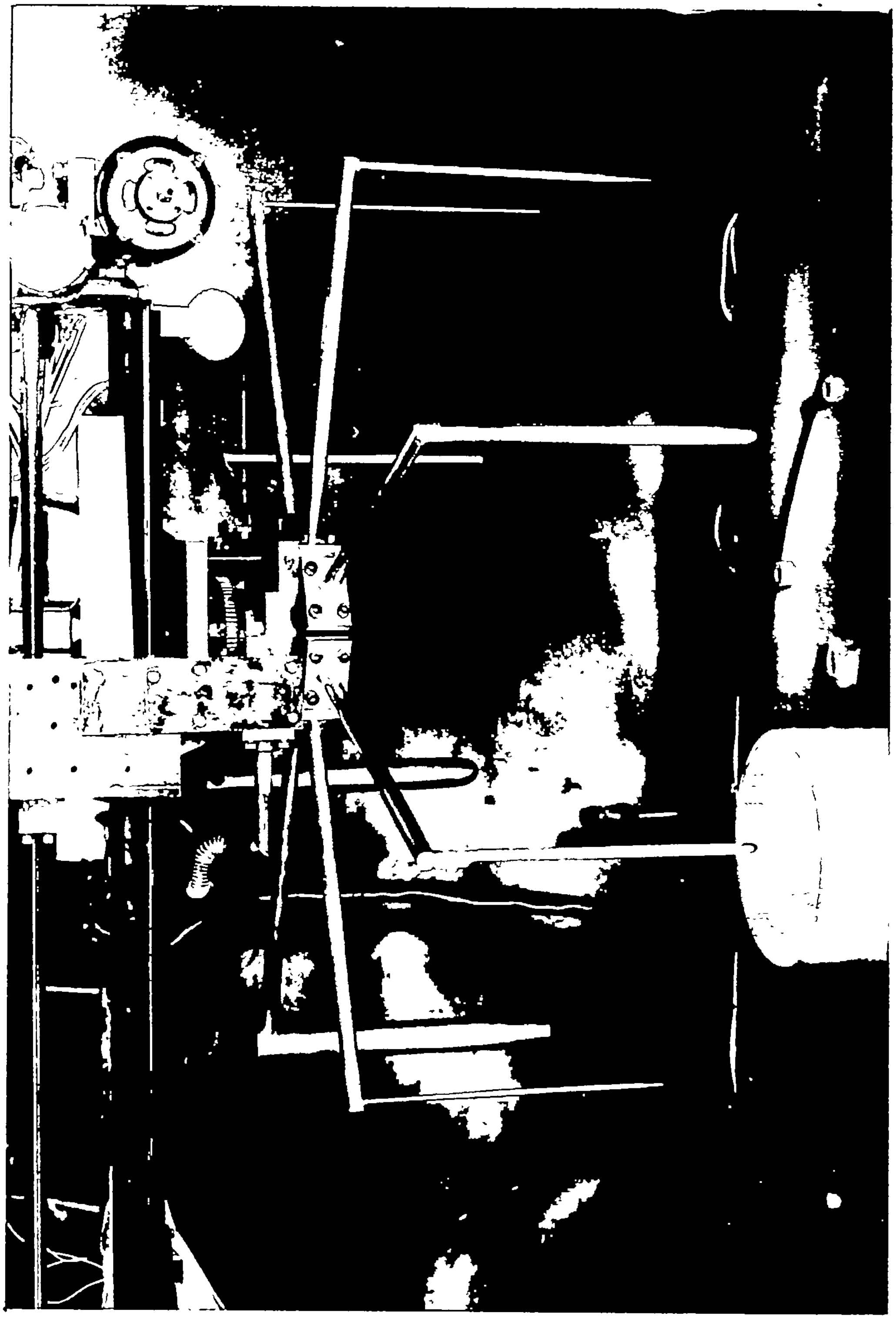

L-80235

Figure 19.- Rotary probe selector.

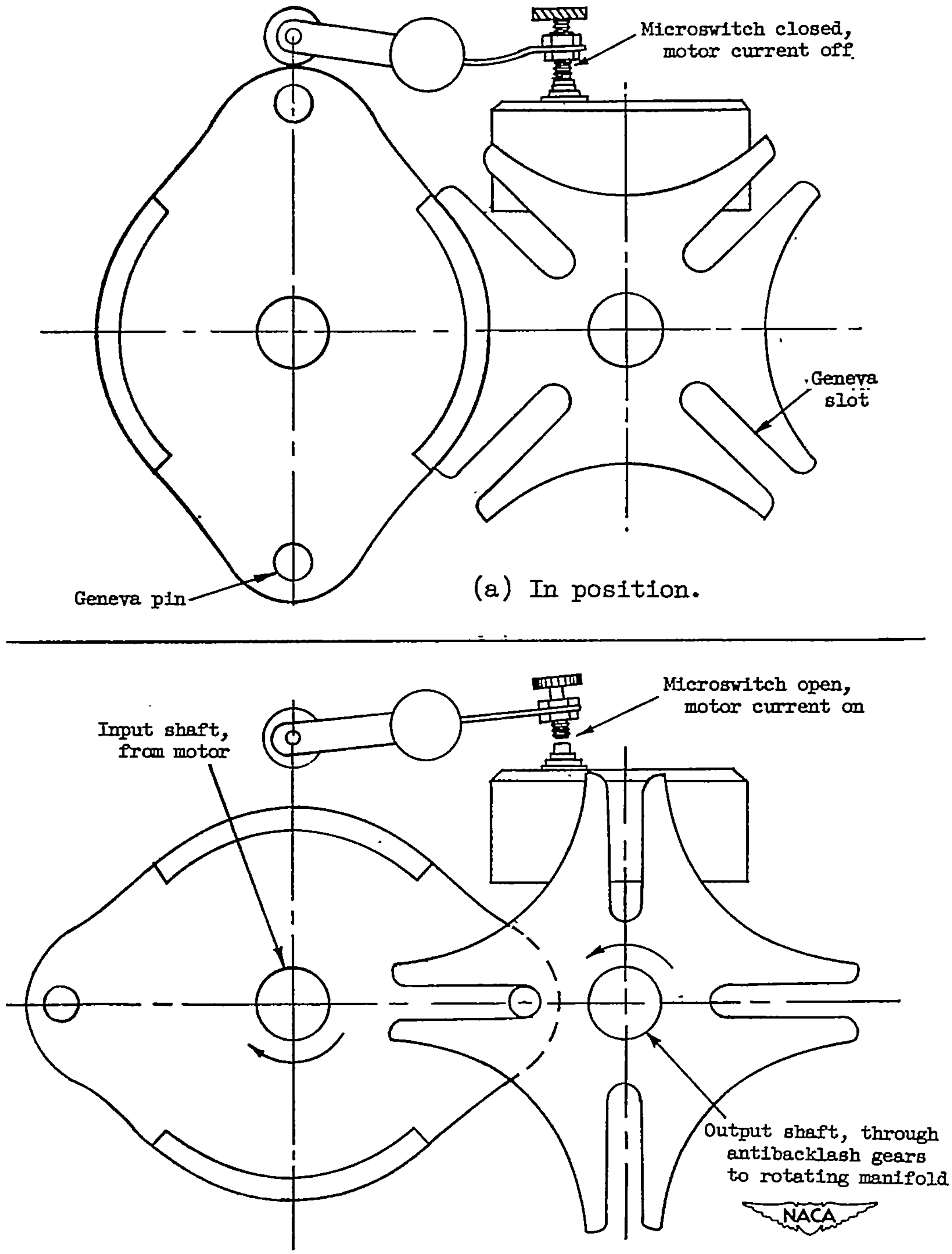

(b) Moving, midway between positions.

Figure 20.- Apparatus for accurately positioning rotating pressure manifold.

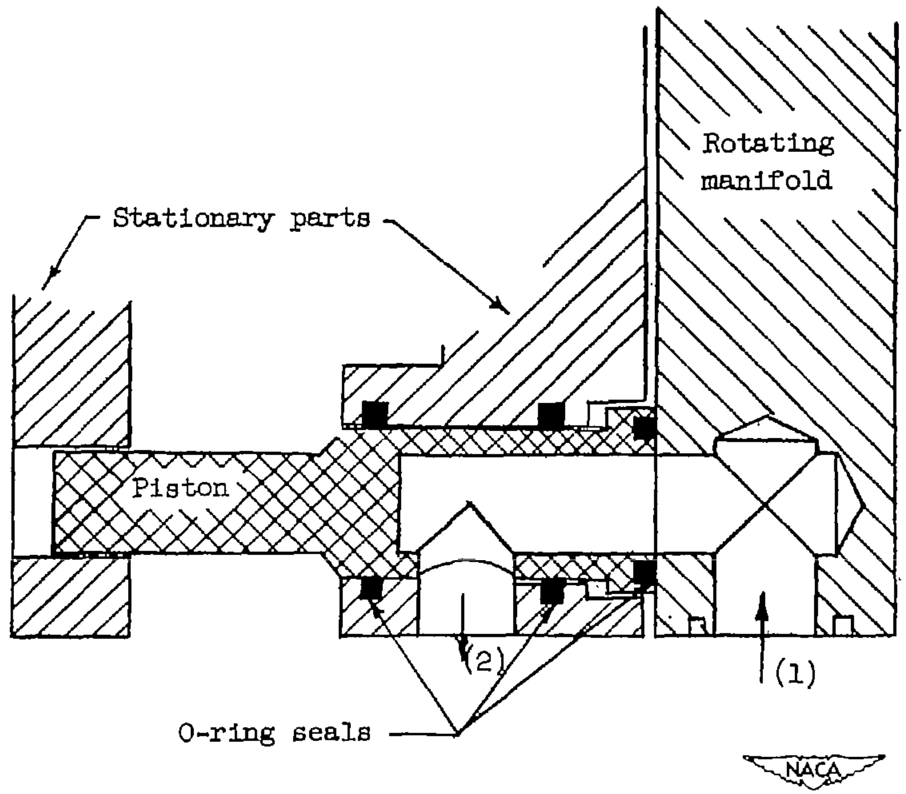

Rotating manifold "in position"
(1) Pressure lead from probe
(2) Pressure lead to manometer

Figure 21.- Schematic sketch of sealing arrangement on rotary probe selector.

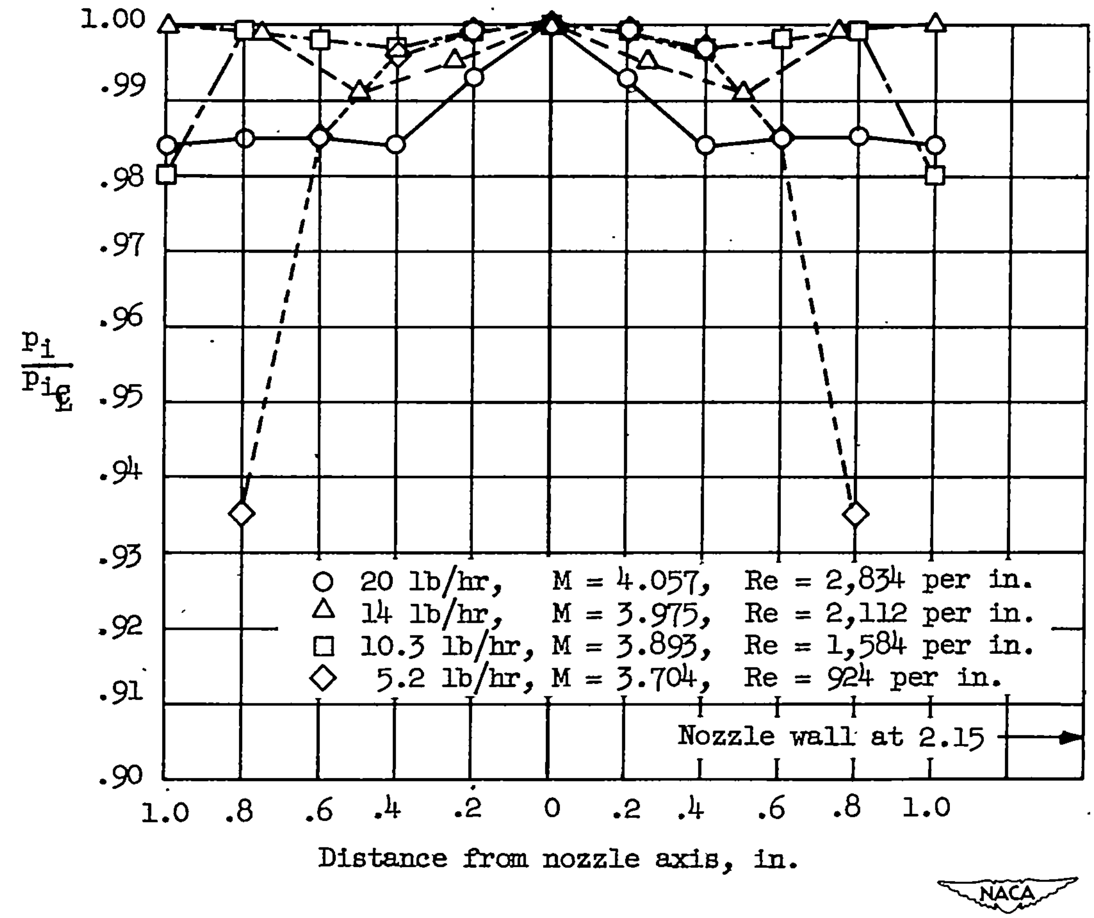

Figure 22.- Radial distribution of impact pressures in nozzle 8.

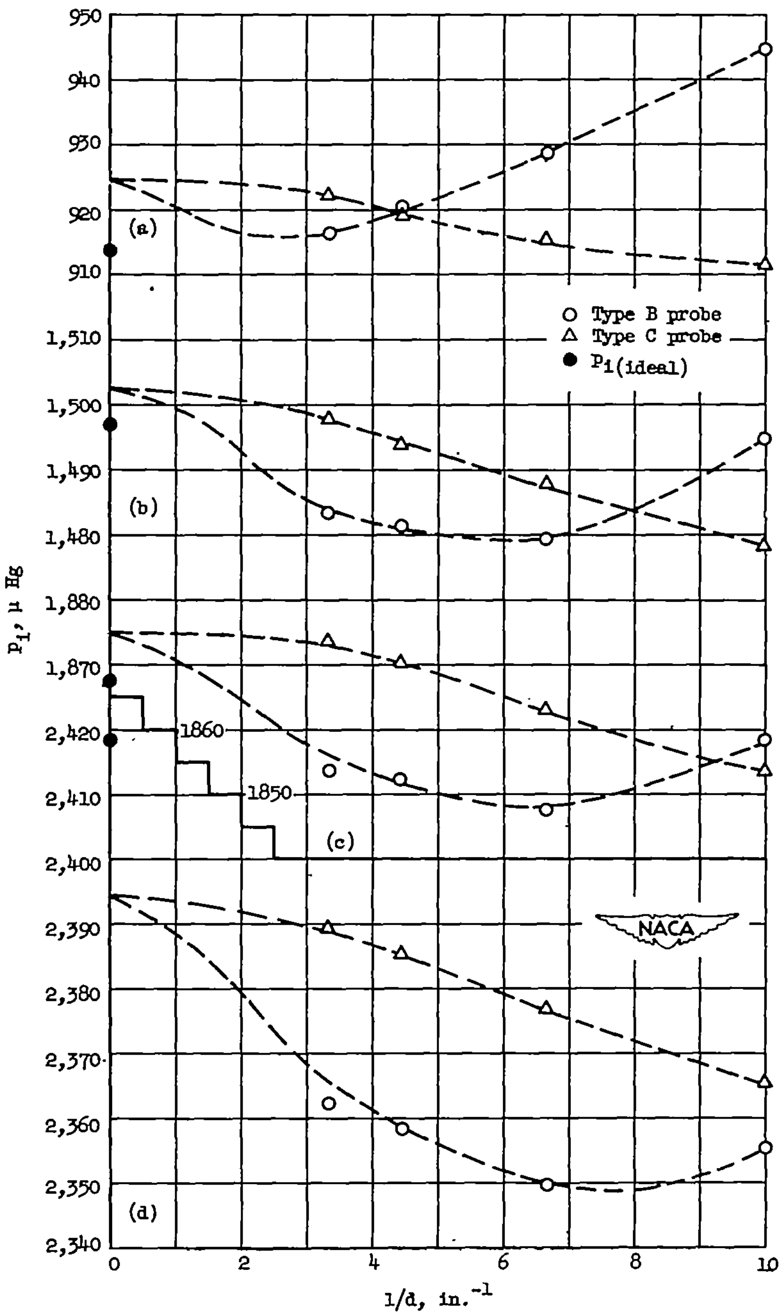

(a) 5.2 pounds per hour; M = 3.704; Re = 924 per inch.

(b) 10.3 pounds per hour; M = 3.893; Re = 1,627 per inch.

(c) 14 pounds per hour; M = 3.975; Re = 2,112 per inch.

(d) 20 pounds per hour; M = 4.057; Re = 2,834 per inch.

Figure 23.- Data from nozzle 8 with probes 0.300 inch off nozzle axis.

NACA-Langley - 9-8-53 - 1000